Probing the Mott physics in -(BEDT-TTF)$_2$X salts via thermal expansion

2015 J. Phys.: Condens. Matter 27 053203

(http://iopscience.iop.org/0953-8984/27/5/053203)

IOP Publishing Journal of Physics: Condensed Matter
J. Phys.: Condens. Matter **27** (2015) 053203 (27pp) doi:10.1088/0953-8984/27/5/053203

Probing the Mott physics in κ-(BEDT-TTF)$_2$X salts via thermal expansion

Mariano de Souza[1,2,4] **and Lorenz Bartosch**[3]

[1] Departamento de Física, Instituto de Geociências e Ciências Exatas—IGCE, Unesp—Universidade Estadual Paulista, Cx. Postal 178, 13506-900 Rio Claro (SP), Brazil
[2] Physikalisches Institut, Goethe-Universität, Max-von-Laue-Str. 1, 60438 Frankfurt am Main, Germany
[3] Institut für Theoretische Physik, Goethe-Universität, Max-von-Laue-Str. 1, 60438 Frankfurt am Main, Germany

E-mail: mariano@rc.unesp.br and lb@itp.uni-frankfurt.de

Received 2 October 2014, revised 25 November 2014
Accepted for publication 5 December 2014
Published 21 January 2015

Abstract

In the field of interacting electron systems the Mott metal-to-insulator (MI) transition represents one of the pivotal issues. The role played by lattice degrees of freedom for the Mott MI transition and the Mott criticality in a variety of materials are current topics under debate. In this context, molecular conductors of the κ-(BEDT-TTF)$_2$X type constitute a class of materials for unraveling several aspects of the Mott physics. In this review, we present a synopsis of literature results with focus on recent expansivity measurements probing the Mott MI transition in this class of materials. Progress in the description of the Mott critical behavior is also addressed.

Keywords: Mott insulators, Mott criticality, lattice effects

(Some figures may appear in colour only in the online journal)

1. Introduction

A tiny change in physical parameters can sometimes have dramatic consequences. This is particularly true in correlated condensed matter systems in which a small alteration in pressure, chemical composition, or temperature can tune a system across a phase transition. In this context, the Mott metal-to-insulator (MI) transition represents one of the most remarkable examples of electronic correlation phenomena. In contrast to conventional band insulators in which all bands are either filled or empty, the Mott insulating state is driven by interactions and emerges once the ratio of the electron–electron interaction U to the hopping matrix element (kinetic energy) t exceeds a critical value. It is essentially this ratio which is tuned in many experiments. Molecular conductors of the κ-phase of (BEDT-TTF)$_2$X (where BEDT-TTF refers to bisethylenedithio-tetrathiafulvalene, i.e. $C_{10}S_8H_8$ and X to a monovalent counter anion), usually called charge-transfer salts, have been recognized as model systems to investigate electronic correlations in two dimensions. In particular, single crystals of wholly deuterated charge-transfer salts of the κ phase with X = Cu[N(CN)$_2$]Br have been attracting broad interest due to fact that they lie in the vicinity of a first-order phase transition line in the phase diagram [1], which separates the metallic from the insulating state, thus giving the possibility of investigating the Mott MI transition using temperature as a tuning parameter. One result to be discussed in detail in the frame of this paper refers to the first experimental observation of the role played by lattice degrees of freedom for the Mott MI transition in the above-mentioned materials [2]. Both the discontinuity and the anisotropy of the lattice parameters observed via high-resolution thermal expansion experiments indicate a complex role of the lattice effects at the Mott MI transition for the κ-(BEDT-TTF)$_2$X charge-transfer salts, which cannot be interpreted simply by taking into account a purely 2D electronic model. Furthermore, in the frame of the present work, a model based on the rigid-unit modes scenario is proposed to describe the negative thermal expansion above the so-called glass-like transition temperature $T_g \simeq 77$ K in deuterated charge-transfer salts of κ-(BEDT-TTF)$_2$Cu[N(CN)$_2$]Br and parent compounds.

[4] Current address: Institute of Semiconductor and Solid State Physics, Johannes Kepler University Linz, 4040 Linz, Austria.

From a theoretical point of view, perturbative approaches and their generalizations are restricted to the regimes $U \ll t$ and $t \ll U$ and have difficulties in addressing phase transitions. In fact, they entirely fail in addressing the critical behavior in the immediate vicinity of a putative critical point. Instead, it is advantageous to start from the critical point itself and use concepts of scaling to describe its vicinity. We will review here how some aspects of the lattice response observed in [2] and [3] can be understood in terms of such a scaling theory [4, 5].

The compound κ-(BEDT-TTF)$_2$Cu$_2$(CN)$_3$ is another material which attracted great interest in the last few years, see, for instance [6] and references cited therein. This system has an almost perfect quasi-2D frustrated triangular lattice with a ratio of hopping integrals close to $t'/t \simeq 1$. Interestingly enough, while the ratio U/t shows a monotonic temperature dependence, the degree of frustration t'/t as a function of temperature presents a non-monotonic behavior and becomes more pronounced at low temperatures [7].

Up to now, no clear experimental evidence of magnetic ordering in κ-(BEDT-TTF)$_2$Cu$_2$(CN)$_3$ has been reported in the literature [8]. Thus, this system has been recognized as a candidate for the realization of a spin-liquid [9]. At $T = 6$ K, a crossover from a paramagnetic Mott insulator to a genuine *quantum spin-liquid* has been proposed [6]. Nevertheless, the physical nature of such a crossover, sometimes called *hidden ordering*, is still controversial. Expansivity measurements performed on this material revealed a pronounced phase-transition-like-anomaly at $T = 6$ K, which coincides nicely with specific heat results reported in the literature [6]. These results provide strong evidence that this lattice instability at $T = 6$ K is directly linked to the proposed spin-liquid phase.

The electronic properties of κ-(BEDT-TTF)$_2$X charge-transfer salts have been reported in various review articles, see, for instance [10–24]. Here we focus on topics linked to dilatometric studies of the κ-(BEDT-TTF)$_2$X salts. Some parts of this review are based on the Ph.D. thesis of one of us [3]. Before giving a detailed outline of the main body of this review article at the end of this introductory chapter, let us first briefly review some general properties of the κ-(BEDT-TTF)$_2$X salts and discuss their crystallographic structure in section 1.1, their phase diagram in section 1.2 and the most relevant experimental results from the literature related to this work in section 1.3.

1.1. The (BEDT-TTF) molecule and crystallographic structure of the κ-ET salts

The basic entity which furnishes the structure of the present class of organic conductors is the (BEDT-TTF) molecule, usually abbreviated simply to ET. The structure of the ET molecule is shown in figure 1. As a result of the two distinct possible configurations of the ethylene end groups in their extremes (known as staggered and eclipsed configurations), the ET molecule is not completely planar. It has been proposed that the degrees of freedom of the ethylene end groups can influence the electronic properties of the salts of the κ-family, see [25] and references cited therein. Employing infra-red imaging spectroscopy, the authors of [26] reported on the sensitivity of the vibration mode of the central C=C bonds, the so-called $a_g(\nu_3)$ mode, upon going from the metallic to the insulating state.

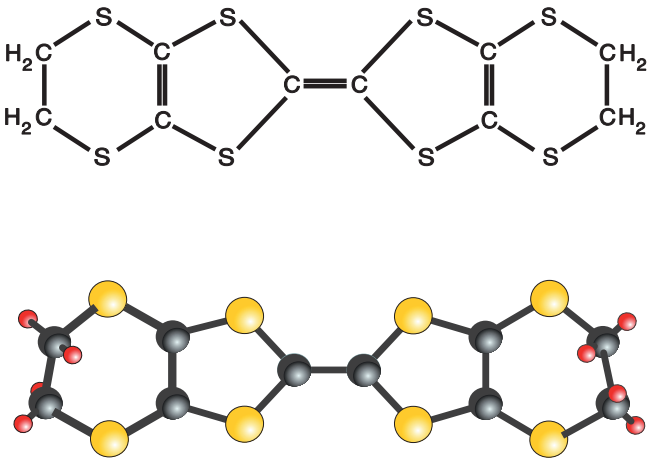

Figure 1. (BEDT-TTF), or simply ET, molecule, which is the basic entity that furnishes the quasi-2D (BEDT-TTF)-based charge-transfer salts. Figure reproduced with permission from [15].

In the following, let us briefly discuss the various phases in which ET charge-transfer salts can crystallize.

During the crystallization process of the (ET)$_2$X salts, the ET molecules can assume different spatial arrangements, giving rise to different phases. Several thermodynamically stable phases, usually referred to by the Greek letters α, β, θ, λ and κ, are known, see figure 2 for a schematic representation of the main known phases. This review is focussed on salts of the κ-phase family. Interestingly enough, different crystalline arrangements imply different band fillings and consequently different physical properties. A detailed discussion about each phase is presented in [21, 22].

The packing pattern of the κ-phase differs distinctly from the others in the sense that it consists of two face-to-face ET molecules, see figure 2. The two molecules interact with each other via overlap between the highest occupied molecular orbitals (HOMOS), as the HOMOS of each molecule are partially occupied [21].

Due to the intrinsic strong dimerization in the κ-(ET)$_2$X family, pairs of ET molecules can be treated as a dimer unity. As a result of such an assumption, an anisotropic triangular lattice is built by such dimer units as shown in figure 3 and the system can be described by the Hubbard model. The counter anion X governs the ratio between the inter-dimer transfer integrals t and t'. For example, for the κ-(ET)$_2$Cu$_2$(CN)$_3$ salt $t'/t = 0.83$ [28, 29], suggesting a strongly frustrated triangular lattice in this compound, to be discussed in more detail below.

It is well to note that, more recently, a new phase, called mixed phase, with alternating α- and κ-type arrangements of the ET molecules, has been synthesized [30]. In addition, a dual-layered superconductor with alternating α'- and κ-type packing has been reported in the literature [31].

The crystallographic structure of the κ-(ET)$_2$Cu[N(CN)$_2$]Br salt [32] is displayed in figure 4. The structure of the latter substance is orthorhombic with the space group *Pnma* with

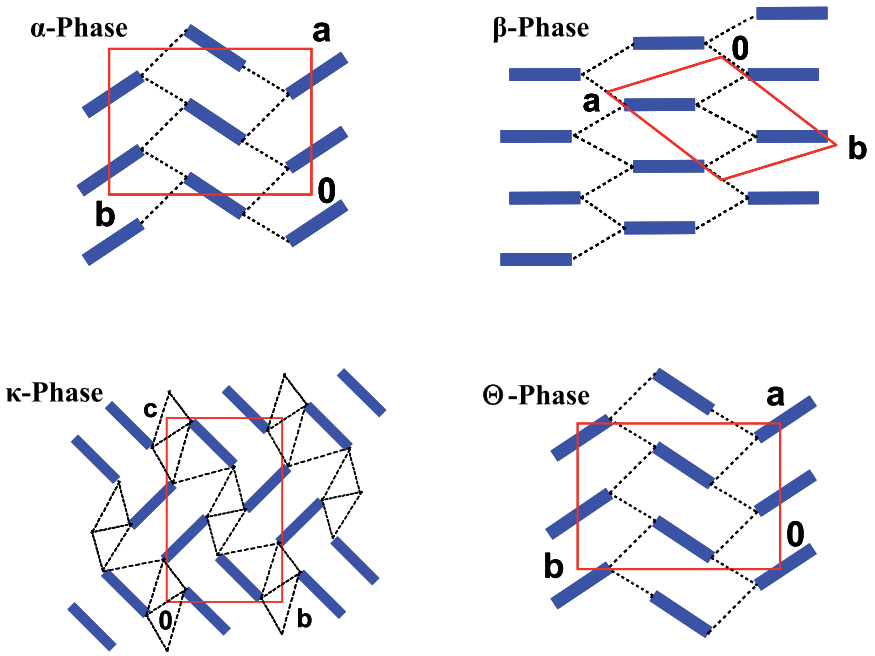

Figure 2. Schematic top view, i.e. view along the ET molecule long axis of the α-, β-, κ- and θ-phase of the ET-based organic conductors. The ET molecules and the unit cells are, respectively, illustrated by solid blue and open red rectangles. The dashed lines indicate the π-orbital overlaps. Figure reproduced with permission from [27].

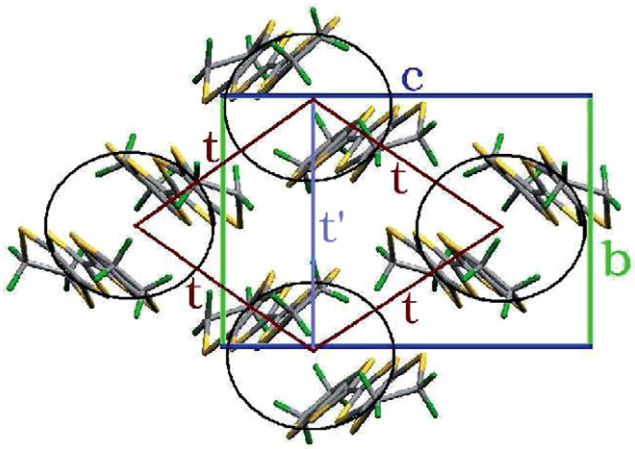

Figure 3. Crystal structure of the κ-$(ET)_2X$ salts (top view). The largest hopping terms between the dimers are indicated by t and t'. Note that the hopping terms t, t' and t form a triangular lattice. It should be noted that the axes labeling refers to the monoclinic lattices, e.g. the salts with X = $Cu(NCS)_2$ or $Cu_2(CN)_3$. Figure taken from [21].

four dimers and four anions in a unit cell. An interesting aspect is that although the compounds κ-$(ET)_2Cu(NCS)_2$ and κ-$(ET)_2Cu_2(CN)_3$ [33] also belong to the κ-phase family, their crystallographic structure is monoclinic. Since the counter anion $X^- = Cu[N(CN)_2]Br^-$ assumes a closed-shell configuration, metallic properties are observed only within the ET layers, which lie in the crystallographic *ac*-plane and correspond to the large face of the crystal. In the perpendicular direction to the referred layers, i.e. the *b*-direction[5], the insulating anion layer partially blocks charge transfer, so that the electrical conductivity along this direction ($\perp$ to the layers)

[5] For the κ-$(ET)_2Cu_2(CN)_3$ salt, the *a*-axis is the out-of-plane direction.

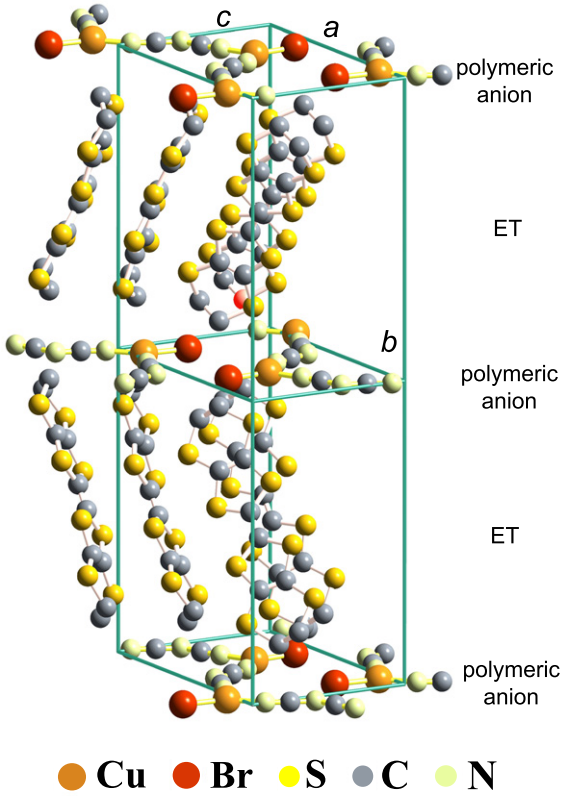

Figure 4. The crystallographic structure of κ-$(ET)_2Cu[N(CN)_2]Br$. While *a* and *c* are the in-plane axes, *b* is along the out-of-plane direction. 'ET' and 'polymeric anion' indicate layers of ET molecules and anions, respectively. The various atoms are represented by different colors, as indicated in the label. For clarity, protons at the end of the ET molecules are omitted. Figure taken from [3].

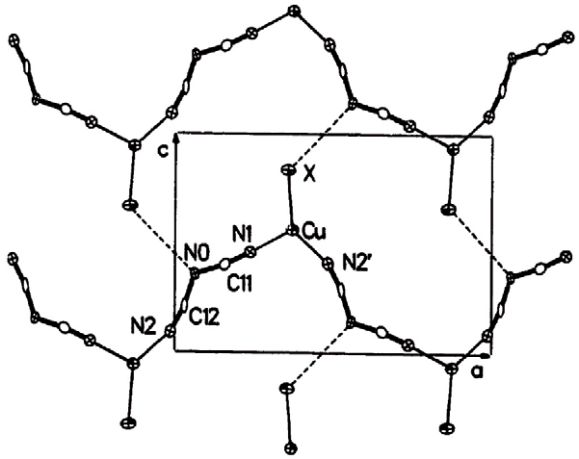

Figure 5. Layered structure formed by the $Cu[N(CN)_2]X^-$ polymeric anion in κ-$(ET)_2Cu[N(CN)_2]X$, view along the b-axis. Here, X refers to either Br or Cl. Dashed lines highlight the X...N weak contacts between the anion chains. The rectangle indicates the contour of the unit cell. Figure reprinted from [34]. Copyright 1991, with permission from Elsevier.

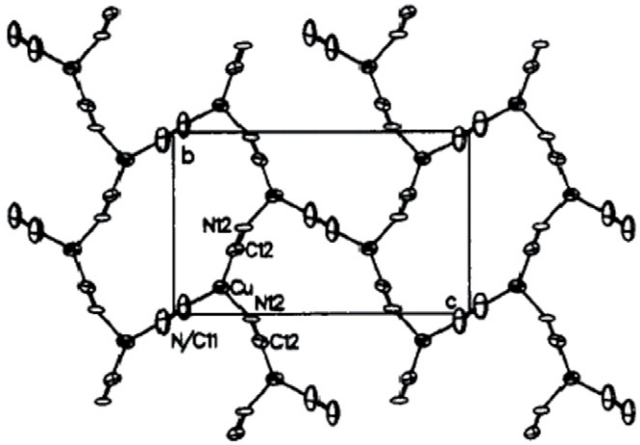

Figure 6. View along the out-of-plane direction (a-axis) of the polymeric anion layer of $Cu_2(CN)_3^-$ in κ-$(ET)_2Cu_2(CN)_3$. The rectangle indicates the contour of the unit cell. The N/C11 cyanide ion is located on an inversion center, being thus crystallographically disordered. The ellipsoids therefore represent either a carbon or a nitrogen atom with a 50% probability. Figure reprinted from [33]. Copyright 1991 American Chemical Society.

is reduced by a factor of 100–1000, depending on the counter anion. Due to this anisotropy, these materials are called quasi-two-dimensional (quasi-2D) conductors.

As displayed in figure 5, the $Cu[N(CN)_2]Br^-$ (or $Cu[N(CN)_2]Cl^-$) polymeric anion structure is composed of planar triply-coordinated Cu(I) atoms with two bridging dicyanamide $[(NC)N(CN)]^-$ ligands, forming a zig-zag pattern chain along the a-axis. The terminal Br^- ions, which overlap slightly with the central N atoms of neighboring polymeric chains, make the third bond at each Cu(I) atom [10].

As shown in figure 6, the counter anion $Cu_2(CN)_3^-$ differs distinctly from the $Cu[N(CN)_2]Br^-$ anion in that it does not form chains, but a planar reticule of Cu(I) ions coordinated in a triangular fashion and bridging cyanide groups. Notably, one of the cyanide groups (labeled N/C11 in figure 6) is located on an inversion center and therefore must be crystallographically disordered [33]. As will be discussed in section 5, this particular arrangement is likely to be responsible for the absence of the so-called glass-like transition in κ-$(ET)_2Cu_2(CN)_3$.

Directional-dependent thermal expansion experiments, to be discussed in section 3, will show that the more pronounced lattice effects, associated with the Mott MI transition for κ-D8-Br, occur along the in-plane direction which is parallel to the anion chains direction (a-axis). In addition, we will propose a model based on the collective vibration modes of the CN groups of the polymeric anion chains to explain the negative thermal expansion along the a-axis above $T_g \simeq 77$ K.

For completeness, the lattice parameters of the κ-$(ET)_2X$ charge-transfer salts discussed in this work are listed in table 1.

1.2. Phase diagram of κ-$(ET)_2X$

Charge-transfer salts of the κ-$(ET)_2X$ family have been recognized as strongly correlated electron systems. Among other features, the latter statement is based on the unusual metallic behavior inherent to these systems, as will be discussed below. Band structure calculations suggest that these materials should be metals down to low temperatures [21]. However, due to correlation effects, the phase diagram embodies various phases, including the paramagnetic Mott insulator (PI), the antiferromagnetic Mott insulator (AF), the superconductor and the anomalous metal, see the phase diagram depicted in figure 7.

A remarkable feature is the competition between antiferromagnetic ordering and superconductivity. The similarities between the present charge-transfer salts and the high-T_c cuprate superconductors have been discussed, see e.g. [14, 36, 37]. The major difference, however, between these two classes of materials is that while for the cuprate superconductors one deals with a *doping-controlled* Mott transition, for the charge-transfer salts to be discussed here one has a *bandwidth-controlled* Mott transition. In addition, no spin-glass phase is observed in organic conductors between the antiferromagnetic and superconducting phases. The symmetry of the superconducting order parameter in these materials is still a topic of debate, see e.g. [38] and references therein. From the experimental point of view, a remarkable feature is the tunability of such systems. In contrast to the cuprate superconductors, where the ground states are tuned by doping, i.e. band filling and therefore disorder is unavoidable, the ground states of organic conductors can be tuned by chemical substitution, namely counter anion substitution and/or by applying external pressure. Pressure mainly induces strain which in turn leads to modified hopping matrix elements t and t' and thereby modifies the bandwidth W. As a consequence, applying pressure leads to a change of the ratio W/U. A pressure of a few hundred bar, which is easily attainable by employing the ^{4}He-gas pressure technique, is enough to make a wide sweep over relevant regions of the pressure versus temperature (P-T) phase diagram[6].

[6] For the Mott insulator V_2O_3, for example, a pressure of a few kbar is required to cross the first-order line in the P–T phase diagram [127].

Table 1. Lattice parameters at room temperature and structure of the investigated κ-$(ET)_2X$ salts [33, 34].

Anion	a (Å)	b(Å)	c(Å)	V(Å^3)	α	β	γ	Struc.
D8-Br	—	—	—	—	⊥	⊥	⊥	Orth.
H8-Br	12.949	30.016	8.539	3317	⊥	⊥	⊥	Orth.
H8-Cl	12.977	29.977	8.480	3299	⊥	⊥	⊥	Orth.
CuCN	16.117	8.5858	13.397	1701.2	⊥	113.42°	⊥	Monoc.

Note: CuCN refers to $Cu_2(CN)_3$. Data for κ-D8-Br are not available in the literature. ⊥ corresponds to 90°. Note that in contrast to the other compounds, for the $Cu_2(CN)_3$ salt the a-direction is the out-of-plane direction.

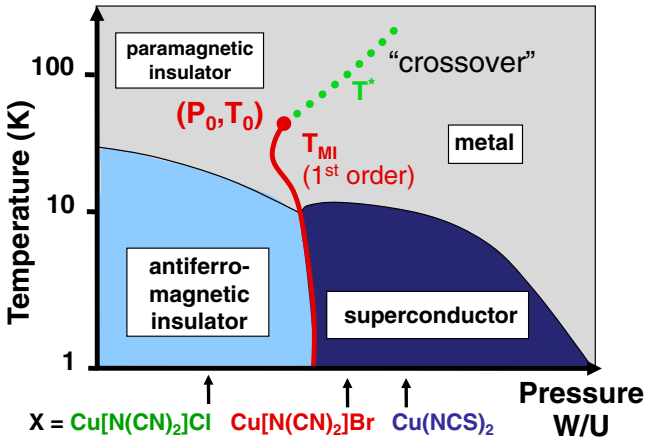

Figure 7. Conceptual pressure versus temperature (P-T) phase diagram for the κ-$(ET)_2X$ charge-transfer salts, after [35]. Arrows pinpoint the positions of the various salts with their counter anion X at ambient pressure. The ratio of the on-site Coulomb repulsion relative to the bandwidth, i.e. U/W, is reduced by application of hydrostatic pressure.

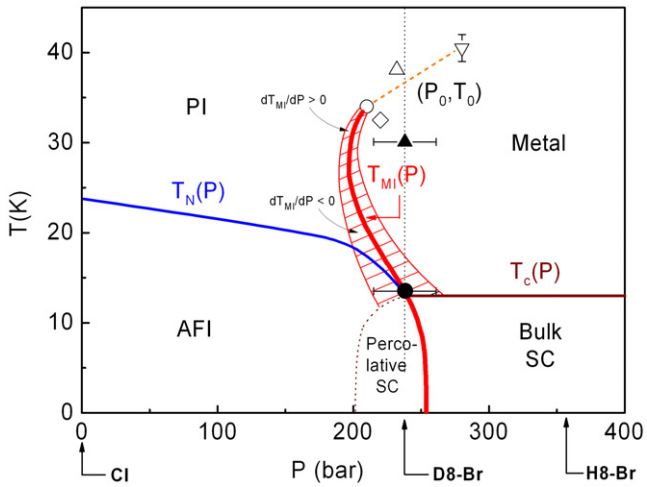

Figure 8. Pressure versus temperature phase diagram of κ-$(ET)_2Cu[N(CN)_2]Z$, with Z = Br or Cl. Lines indicate the respective phase transitions. D8-Br and H8-Br indicate the positions (estimated according to [43]) of the κ-D8-Br and κ-H8-Br salts, respectively. The orange broken line indicates the crossover from the metallic to the insulating regime above the critical temperature. Thin solid lines (red), demarcating the hatched area, refer to the positions of the anomalies observed via ultrasonic measurements (see figure 10). The vertical (black) dotted line indicates T sweeps of the κ-D8-Br salt, depicting a crossing of the S-shaped first-order Mott MI phase transition line. PI, AFI and SC denote the paramagnetic insulator, the antiferromagnetic insulator and the superconducting phase, respectively. The open circle refers to the Mott critical end point. At the point marked by a closed circle in the phase diagram, T_{MI} matches T_N, see the discussion in section 3.2. As can be seen in the figure, the slope of dT_{MI}/dP can be both positive and negative, indicating that upon crossing the MI line the entropy can either increase or decrease. While the entropy increases for $dT_{MI}/dP > 0$ when crossing the MI line from the metallic to the PI state, for $dT_{MI}/dP < 0$, when going from the metallic to the AFI state, the entropy associated with the metallic state is decreased due to magnetic ordering. Figure taken from [2].

The phase diagram shown in figure 8 has been mapped by NMR and ac susceptibility [39], transport [41] and ultrasonic [42] measurements under helium gas pressure on the salt with X = $Cu[N(CN)_2]Cl$. In this *generic* phase diagram, the antiferromagnetic transition line, not observed in ultra-sound experiments [42], was obtained from the NMR relaxation rate [39]. From the splitting of NMR lines, the estimated magnetic moment per dimer is (0.4–1.0) μ_B. The superconducting transition line was determined from the ac susceptibility [39] and its fluctuations in the immediate vicinity of the Mott transition by means of Nernst effect measurements [40], whereas the S-shaped first-order MI transition line via ultra-sound [42], transport [41] and ac susceptibility [39] measurements.

This first-order Mott MI transition line ends in a critical point (P_0, T_0), which has been studied by several groups [39, 41, 42, 44, 45]. Among possible scenarios, this critical end-point has been discussed in analogy with the liquid-gas transition, see e.g. [46]. In this scenario, above (P_0, T_0) the metallic state cannot be distinguished from the paramagnetic insulating state. More recent studies suggest that lattice effects are relevant close to the Mott critical end-point [2, 4, 5].

By means of resistivity measurements under pressure, the critical behavior in the proximity of the point (P_0, T_0) was investigated by Kagawa *et al* [45]. These authors found critical exponents which do not fit in the most common universality classes and they assigned this to the quasi-2D structure of the present substances. Such a scenario shall be examined in more detail in section 4. The possibility of tuning the system from the insulating to the metallic side of the P versus T phase diagram, i.e. crossing the first-order Mott MI line by application of pressure, is indicative of a bandwidth-controlled Mott MI transition. Owing to the position of the salts with different counter anions X, as shown in figure 8, the fully hydrogenated salt with X = $Cu[N(CN)_2]Br$ superconducts below 12 K, the highest T_c under ambient pressure among all organic conductors till the present date, whereas the salt with counter anion X = $Cu[N(CN)_2]Cl$ is a Mott insulator with $T_N \simeq 24$ K.

It has very recently been shown that the antiferromagnetic Néel state is accompanied by charge ordering, i.e. the salt κ-$(ET)_2Cu[N(CN)_2]Cl$ is in fact a multiferroic [47].

Interestingly enough, fully deuteration of the ethylene end groups of the ET molecules in the salt with $X = Cu[N(CN)_2]Br$, as described in detail above, results in a shift of the latter towards the boundary of the *S*-shaped first-order Mott MI transition line. It is due to their close position to this line [1] that the deuterated salt with $X = Cu[N(CN)_2]Br$, hereafter named κ-D8-Br, has attracted particular interest. As a matter of fact, the C–H and C–D bond lengths are slightly different. It is well known that the deuterium nucleus has one proton and one neutron, while the hydrogen nucleus is formed simply by one proton. Thus deuterium has a higher mass than hydrogen and, as consequence C–D chemical bonds have a smaller eigen-frequency than the C–H bonds. Hence, the displacement of the deuterium atoms from their equilibrium positions during the vibration process is smaller than that estimated for the hydrogen atoms. Thus the C–D chemical bonds are slightly smaller than the C–H bonds. Furthermore, the contact between the $C–D_2$ end groups and the anions is weaker than that between the $C–H_2$ end groups and the anions. As a consequence, the lattice of the fully deuterated salt is softer than the lattice of the fully hydrogenated salt. This process of exchanging atoms is usually called applying 'chemical pressure'. In fact, application of pressure (chemical or external) changes the distance between the ET molecules so that the overlap between π-orbitals' is increased and, as a consequence, the bandwidth *(W)* is changed. The ratio W/U is considered the pivotal parameter which defines the various phases of these substances [35].

Interestingly enough, for the salt with the anion $X = Cu_2(CN)_3$, magnetic ordering is absent in the whole insulating region. The P versus T phase diagram of the κ-$(ET)_2Cu_2(CN)_3$ salt is depicted in figure 9.

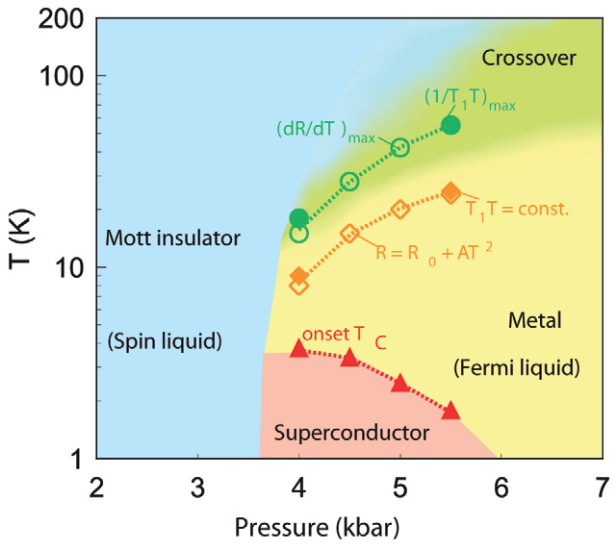

Figure 9. P-T phase diagram of the κ-$(ET)_2Cu_2(CN)_3$ salt, obtained from resistance and NMR measurements under pressure using an oil pressure cell. The Mott MI transition and crossover lines are associated with the temperature at which the quantities spin-lattice relaxation rate divided by temperature $(1/T_1T)$ and dR/dT show a maximum, see labels indicated in the figure. The Fermi-liquid regime (yellow area) was fixed by the temperature regime where the resistance R follows the $R_0 + AT^2$ relation and $(1/T_1T)$ is constant. The superconducting transition line was obtained via in-plane resistance measurements. Reprinted with permission from [48]. Copyright 2005 by the American Physical Society.

1.3. Key experimental results

As mentioned above, the metallic state of κ-$(ET)_2X$ presents some distinct properties as compared to those of conventional metals. For instance, in the κ-H8-Br salt, the out-of-plane resistance as a function of temperature has a non-monotonic behavior [49] with a maximum around 90 K, which was observed to be sample-dependent. Decreasing temperature, this maximum is followed by a sudden drop and the resistivity sharply changes its slope around $T^* \simeq 40$ K. Below $T_c \simeq 11.5$ K superconductivity is observed. On applying pressure, T^* shifts to higher temperatures and disappears at roughly 2 kbar. From about $T^* \simeq 40$ K down to $T_c \simeq 11.5$ K the resistance obeys a T^2 behavior which is frequently assigned to a coherent Fermi liquid state. NMR studies revealed a peak in the spin-relaxation rate divided by temperature $(1/TT_1)$ around T^* for the present compound [50]. The anomalous metallic behavior around T^* was also observed by thermal, magnetic, elastic and optical measurements, see [49] and references therein. The origin of the T^* anomaly is still controversial. Ultrasonic velocity measurements under pressure on the compound κ-$(ET)_2Cu[N(CN)_2]Cl$ performed by Fournier *et al* [42] revealed the existence of two new lines in the phase diagram (not indicated in figure 8) which merge at the critical end point. These lines indicate the softening of the lattice response and should therefore coincide with anomalies expected in future dilatometric studies under pressure. It is important to keep in mind that the two lines observed in ultrasound experiments are different from the metal-to-insulator crossover line above T_c.

The experimental findings obtained by Fournier *et al* are shown in figure 10. From this data set, pronounced anomalies, depending on the pressure, are observed below around 40 K. The maximum amplitude of the softening in the sound velocity (at $T \approx 34$ K, $P \approx 210$ bar) marks the critical end point (P_0, T_0) and corresponds to a softening of roughly 20% of the sound velocity. On increasing the pressure, the peak position shifts its position to higher temperatures. Below P_0 the anomaly becomes gradually less pronounced and saturates at around 32 K. The peak position was thus used by the authors to draw the two *crossover* lines in the P-T phase diagram (see figure 11).

The large anomalies in the sound velocity observed by Fournier *et al* were discussed in terms of a diverging electronic compressibility. As a matter of fact, acoustic and lattice anomalies are, according to dynamical mean-field theory (DMFT) calculations, expected at the Mott MI transition as a reaction to the softening of the electronic channel, see [51, 52]. The explanation for this is that in the metallic state the conduction electrons contribute more to the cohesion of the solid than in the insulating one. Based on this argument, according to [51], as an effect of the localization, abrupt

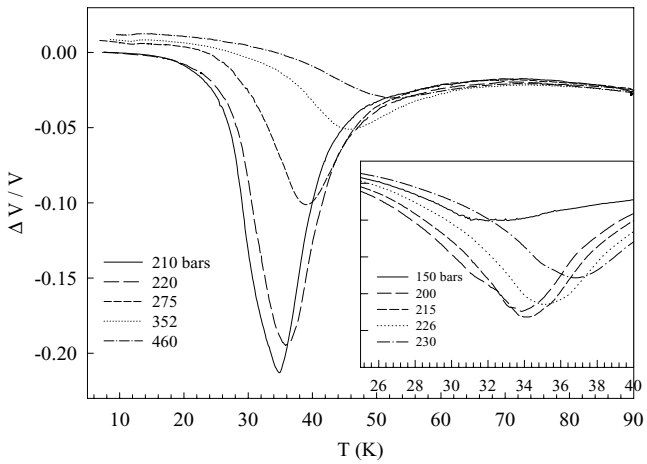

Figure 10. Main panel: Relative sound velocity $\Delta V/V$ versus T under pressure for the κ-$(ET)_2Cu[N(CN)_2]Cl$ salt. The various pressure values are indicated in the label of the figure. Inset: data for pressures below 230 bar. Reprinted with permission from [42]. Copyright 2003 by the American Physical Society.

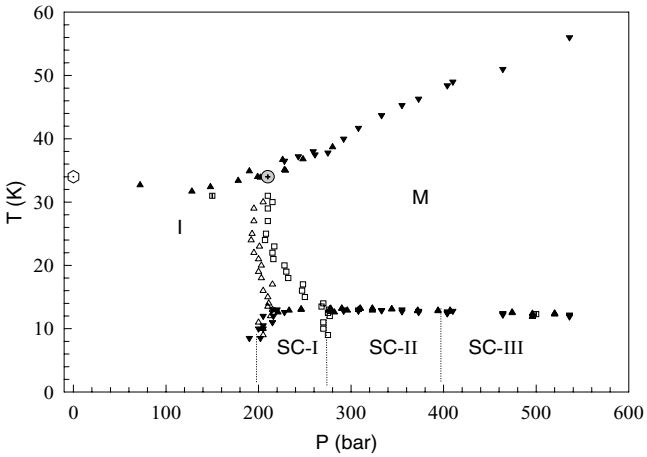

Figure 11. Phase diagram obtained from ultrasound experiments under pressure for the κ-$(ET)_2Cu[N(CN)_2]Cl$ salt. Different symbols refer to the various anomalies observed on three different samples. The critical point (P_0, T_0) is indicated by the gray circle. SC-I and -II indicate metastable superconductivity, while SC-III indicates bulk superconductivity. Dotted hexagon indicates the pressure point, obtained from microwave resistivity measurement at ambient pressure. Reprinted with permission from [42]. Copyright 2003 by the American Physical Society.

changes of the lattice parameters are expected at the Mott MI transition. We shall discuss the lattice effects for the present material in section 3.

Regarding the Fermi surface, the weak interlayer transfer integrals were nicely estimated from magnetoresistance measurements for deuterated κ-$(ET)_2Cu(NCS)_2$ (figure 12).

From a more fundamental point of view, the determination of the interlayer transfer integral in a quasi-2D system is quite helpful, for instance, to understand the validity of the criterion usually adopted to classify whether the interlayer charge transport in quasi-2D systems is incoherent or coherent. For a detailed discussion, see e.g. [53] and references cited therein. Thus charge-transfer salts of the κ-$(ET)_2X$ phase serve as a good platform to investigate the fermiology of quasi-2D systems. Furthermore, knowing precisely the relevant parameters that govern the Mott Physics, theoretical approaches can be employed to understand the fundamental aspects of the Mott transition, see e.g. [7].

Owing to the magnetic properties of the κ-$(ET)_2X$ family, several studies employing different experimental methods have been carried out on the salt with $X = Cu[N(CN)_2]Cl$ [54–56].

By means of resistance measurements, a magnetic-field-induced Mott MI transition was observed by Kagawa *et al* [57] by varying temperature, pressure and the magnetic field. From an analysis of their NMR line shape, relaxation rate and magnetization data, Miyagawa *et al* [56] were able to describe the spin structure of this state. Below $T = 26$–27 K, they found a commensurate antiferromagnetic ordering with a moment of (0.4–1.0) μ_B/dimer, as already mentioned above. The observation of an abrupt jump in the magnetization curves for fields applied perpendicular to the conducting layers, i.e. along the b-axis, was discussed in terms of a spin-flop (SF) transition. Furthermore, a detailed discussion about the SF transition, taking into account the Dzyaloshinskii–Moriya exchange interaction, was presented by Smith *et al* [58, 59]. Similarly to that for the pressurized chlorine salt, a magnetic-field-induced MI transition was also observed in partially deuterated κ-$(ET)_2Cu[N(CN)_2]Br$ [60]. In addition, a discussion on the phase separation and SF transition in κ-D8-Br was reported in the literature [61].

As already mentioned above, the organic charge-transfer salt κ-$(ET)_2Cu_2(CN)_3$ has the peculiarity that the ratio of its hopping matrix elements t' to t is close to unity, more precisely 0.83 [28, 29], leading to a strongly frustrated isotropic $S = 1/2$ triangular lattice with the coupling constant $J = 250$ K, where this coupling constant is obtained by fitting the magnetic susceptibility using the triangular-lattice Heisenberg model. Magnetic susceptibility and NMR measurements revealed no traces of long-range magnetic ordering down to 32 mK [8]. Based on these results, this system has been proposed to be a candidate for the realization of a spin-liquid state [62].

Interestingly, upon applying pressure (see figure 9), the system becomes a superconductor [48], i.e. superconductivity appears in the vicinity of a spin-liquid state. As shown in figure 13, specific heat experiments revealed the existence of a hump at 6 K, insensitive to magnetic fields up to 8 T.

This feature was assigned to a crossover from the paramagnetic Mott insulating to the quantum spin-liquid state [6]. Such a 'crossover' has been frequently referred to as 'hidden ordering'. Below 6 K, the specific heat presents a distinct T-dependence, including a T-linear dependence in the temperature window 0.3–1.5 K, as predicted theoretically for a spin-liquid [63]. The spin entropy in this T-range is roughly 2.5% of $R \ln 2$ [64], indicating that below 6 K only 2.5% of the total spins contribute to the supposed spin-liquid state. Extrapolating the low-T specific heat data, the authors of [6] found a linear specific heat coefficient $\gamma = (20 \pm 5)$ mJ mol^{-1} K^{-2} (see figure 14). The latter is sizable given the insulating behavior of the material and contrasts with a vanishing γ value for the related compounds κ-$(ET)_2Cu[N(CN)_2]Cl$ and fully deuterated κ-$(ET)_2Cu[N(CN)_2]Br$. A finite γ could indicate a spinon Fermi surface.

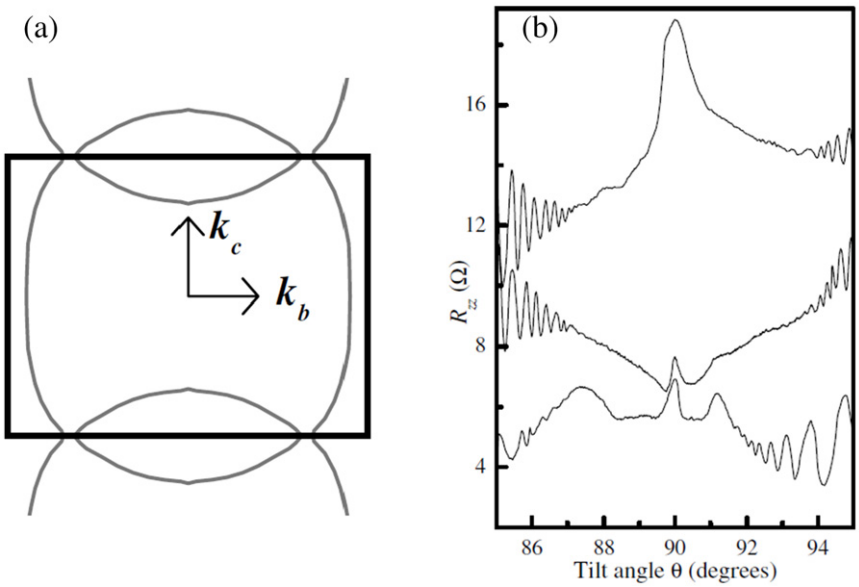

Figure 12. (*a*) Fermi surface cross section and Brillouin zone for κ-$(ET)_2Cu(NCS)_2$. (*b*) Interlayer magnetoresistance R_{zz} for deuterated κ-$(ET)_2Cu(NCS)_2$ as a function of the tilt angle ($\theta \equiv$ angle formed between the applied magnetic field B and the normal to the quasi-2D planes formed by the BEDT-TTF layers) taken under a static magnetic field $B = 45$ T at $T = 520$ mK. The central peak (around $\theta = 90^\circ$) is associated with the closed orbits shown in (*a*), while the features in the edges are due to angle-dependent magnetoresistance oscillations (AMRO). Reprinted with permission from [53]. Copyright 2002 by the American Physical Society.

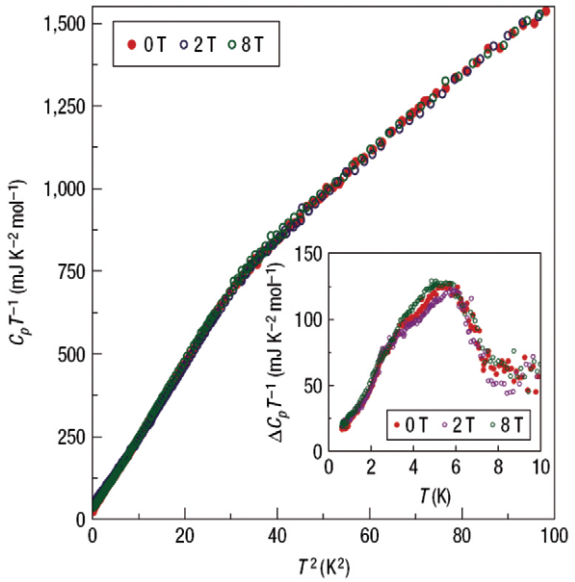

Figure 13. Main panel: specific heat divided by T, i.e. C_p/T, data for the κ-$(ET)_2Cu_2(CN)_3$ salt plotted against T^2 until 10 K. A broad hump anomaly around $T = 6$ K can be clearly observed. Inset: specific heat data for κ-$(ET)_2Cu_2(CN)_3$, assuming that the data of the superconductor κ-$(ET)_2Cu(NCS)_2$ describe the phonon background. Reprinted by permission from Macmillan Publishers Ltd: [6], copyright 2008.

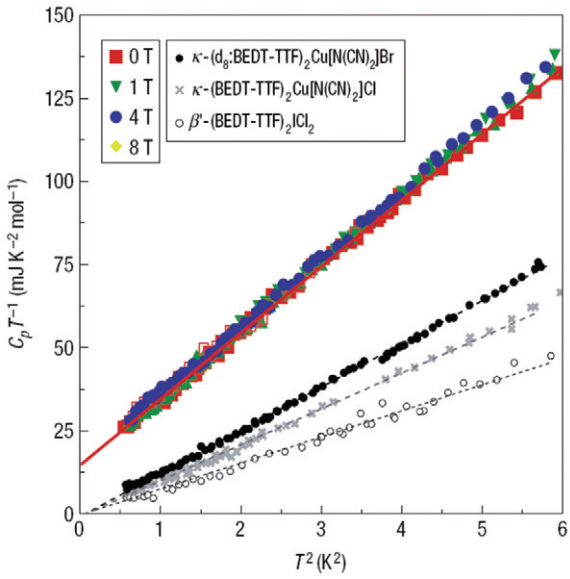

Figure 14. Low-temperature specific heat data for the κ-$(ET)_2Cu_2(CN)_3$ salt as well as κ-D8-Br, κ-$(ET)_2$Cu[N(CN)$_2$]Cl and β'-$(ET)_2I\,Cl_2$, plotted is C_p/T versus T^2. The extrapolation of the red solid line towards zero temperature indicates the existence of a T-linear contribution for the spin-liquid candidate κ-$(ET)_2Cu_2(CN)_3$. Data under magnetic fields for κ-$(ET)_2Cu_2(CN)_3$ are also shown. Reprinted by permission from Macmillan Publishers Ltd: [6], copyright 2008.

A gauge theory with an attractive interaction between spinons mediated via a non-compact $U(1)$ gauge field was proposed by Lee *et al* [65] to describe a possible spin-liquid state in κ-$(ET)_2Cu_2(CN)_3$. Within this model, a pairing of spinons on the same side of the Fermi surface should occur at low temperatures. The attractive interaction between spinons with parallel momenta is quite analogous to Ampère's force law which states that two current carrying wires with parallel currents attract. The authors deduce that the pairing of spinons is accompanied by a spontaneous breaking of the lattice symmetry, which in turn should couple to a lattice distortion (analogously to the Spin-Peierls transition) and should be detectable experimentally via x-ray scattering. While Lee *et al* [65] derive a specific heat which

scales as $T^{2/3}$ and therefore contributes even stronger than linear at low T, it should be kept in mind that the very-low temperature behavior of κ-$(ET)_2Cu_2(CN)_3$ is dominated by a diverging nuclear contribution to the specific heat. Indeed, the data set reported by Yamashita *et al* [6] is also reasonably well described by a $T^{2/3}$ behavior at intermediate temperatures [64].

Even though specific heat measurements by Yamashita *et al* [6] are compatible with a spinon Fermi surface with gapless excitations, thermal conductivity measurements reported by Yamashita *et al* in [66] show a vanishing low-temperature limit of the thermal conductivity divided by temperature, indicating the absence of gapless excitations. The excitation gap was estimated to be $\Delta_\kappa \simeq 0.46$ K. Applying a theory based on Z_2 spin liquids, Qi *et al* argued that thermal transport properties should be dominated by topological vison excitations [67]. The gap found by Yamashita *et al* [66] should therefore be interpreted as a vison gap. It was pointed out by Ramirez [64] that before a final declaration of κ-$(ET)_2Cu_2(CN)_3$ as a spin-liquid is made some points should be clarified, among them the anomaly observed in the specific heat at 6 K. We will come back to the system κ-$(ET)_2Cu_2(CN)_3$ in section 5 where we will discuss its thermal expansion properties. Regarding the fascinating properties of this salt, recently the existence of two magnetic field-induced quantum critical points was reported in the literature [68]. Yet, based on a careful analysis of their muon spin rotation results, performed under extreme conditions, the authors of [68] discuss a possible interpretation for the features observed in several physical quantities around 6 K in terms of the formation of bosonic pairs emerging from a portion of the fermionic spins in κ-$(ET)_2Cu_2(CN)_3$.

The remainder of this article is organized as follows: In section 2, we discuss experimental aspects like sample preparation and high-resolution thermal measurements. Section 3 is dedicated to an exhaustive discussion on the thermal expansivity of fully deuterated salts of κ-$(ET)_2Cu[N(CN)_2]Br$, while in section 4 the Mott criticality is comprehensively reviewed. Section 5 is devoted to the discussion of the thermal expansivity of the spin-liquid candidate κ-$(ET)_2Cu_2(CN)_3$. Finally, conclusions and perspectives are presented in section 6.

2. Experimental setup

2.1. Sample preparation

As thermal expansion measurements under external hydrostatic pressure are extremely challenging, using compounds of different chemical composition currently represents the most practical way to probe the phase diagram of the κ-$(ET)_2X$ family via dilatometry. Deuterated (98%) bis(ethylenedithiolo)-tetrathiofulvalene (D8-ET) was grown according to Hartke *et al* [69] and Mizumo *et al* [70], making the reduction of carbon disulfide with potassium in dimethylformamide and subsequent reaction with deuterated (98%) 1.2-dibromoethane. The intermediate thione $C_5D_4S_5$ was mixed with triethylphosphite in an inert atmosphere kept at 1200 °C and recrystallized several times from chlorobenzene. By investigating the CH_2 and CD_2 stretch vibration modes, no signs of any CH_2 or CDH vibrations could be detected, see [71]. Hence, the grade of deuteration of κ-$(D8\text{-}ET)_2Cu[N(CN)_2]Br$ is at least 98% [72]. As discussed in detail in [49], by employing the preparation technique described above, hydrogenated single crystals of the same substance resulted in samples whose resistivity revealed reduced inelastic scattering and enhanced residual resistivity ratios. In general, the crystals have bright surfaces in shapes of distorted hexagons with typical dimensions of approximately $1 \times 1 \times 0.4$ mm^3. Due to the small size and fragility of the crystals, the experimental challenge lies in assembling them in the dilatometer. The samples of the deuterated and hydrogenated variants of κ-$(ET)_2Cu[N(CN)_2]Br$ and κ-$(ET)_2Cu_2(CN)_3$ salts used for measurements discussed in this work are listed in table 2. The fully deuterated (hydrogenated) salts of κ-$(ET)_2Cu[N(CN)_2]Br$ will be subsequently referred to as κ-D8-Br (κ-H8-Br). Samples of κ-$(ET)_2Cu_2(CN)_3$ studied here were prepared according to [33].

Table 2. Samples of the organic conductor κ-$(ET)_2X$ on which thermal expansion measurements were performed. Crystal #4 was used to perform preliminary studies of Raman spectroscopy. In [2] crystal #2 is referred to as crystal #3.

Anion X	Crystal Number	Direction	Batch
D8-Br	1	a, b, c	A2907[a]
D8-Br	2	a, b	A2995[a]
D8-Br	3	a, b, c	A2907[a]
D8-Br	4	—	A2907[a]
H8-Br	7	b	A2719[a]
H8-$Cu_2(CN)_3$	1	a	SKY 1050[b]
H8-$Cu_2(CN)_3$	1	c	KAF 5078[b]
H8-$Cu_2(CN)_3$	2	b	KAF 5078[b]

[a] Refers to samples provided by Schweitzer (University of Stuttgart).
[b] To samples provided by Schlueter (Argonne National Laboratory).

2.2. Thermal expansion measurements

As already mentioned in the introduction, thermal expansion coefficient measurements are a very useful and powerful tool to explore phase transitions in solid state physics research [3, 4, 47, 73–85]. For instance, combining specific heat and thermal expansion data one can employ the Ehrenfest relation to determine the pressure dependence of a second-order phase transition temperature. Such an analysis may serve also as a check of its direct measurement as a function of hydrostatic pressure. Furthermore, contrasting with specific heat which is an isotropic property, anisotropic effects may be studied via thermal expansion measurements. Regarding the charge-transfer salts of the κ-phase, to our knowledge, the first high-resolution thermal expansion experiments along the three crystallographic directions were carried out about twenty years ago by Kund and collaborators [86].

The measurements presented in the present work were carried out by making use of an ultra-high-resolution capacitance dilatometric cell, built after [87], with a maximum resolution of $\Delta l/l = 10^{-10}$, in the temperature range 1.3

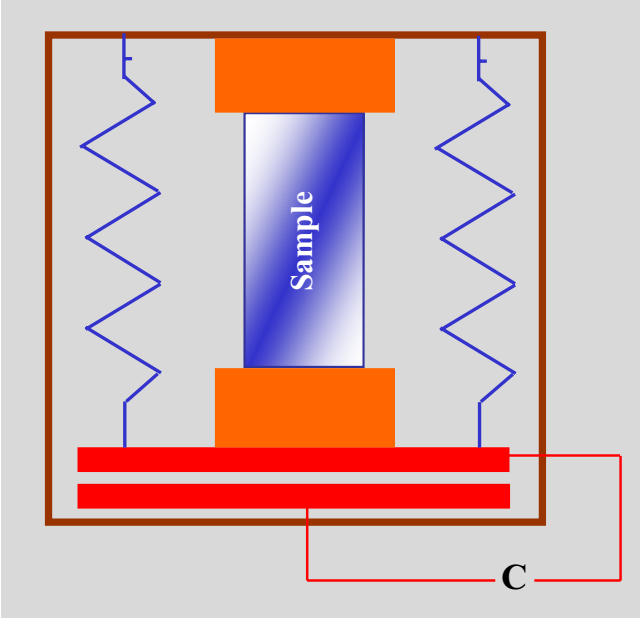

Figure 15. Schematic representation of the cell used for the thermal expansion measurements. Details are discussed in the main text. Figure adapted from [3].

(pumping of Helium bath) to 200 K under magnetic fields up to 10 T. In order to avoid external vibrations, the cryostat is equipped with shock absorbers. A detailed description of the dilatometer used in this work has been presented in several works [90–92]. The principle of measurement is described in the following. As sketched in figure 15, the cell, which is entirely made of high-purity copper to ensure good thermal conductivity and covered with gold is constituted basically of a frame (brown line) and two parallel pistons (orange), the upper one being movable. As a matter of fact, the gold layer should work like a protection, avoiding oxidation of the cell. Nevertheless, after some years in use, two striking anomalies have been observed at $T \simeq 212$ K and 230 K. These anomalies are assigned to the formation of copper-oxide (CuO) [93] in the body of the cell. Due to this, experimental data taken in this T window are not reliable.

The sample is placed between these two pistons and by moving the upper piston carefully, the starting capacitance is fixed. The lower piston is mechanically linked to a parallel plate capacitor, as schematically represented by springs in figure 15. The variation of the sample length, i.e. contraction or expansion, as the temperature is lowered or increased, together with cell effects corresponds exactly to the change of the distance between the plates of the capacitor and consequently to a change of the capacitance, so that very tiny length changes can be detected. In this construction, the distance between the plates of the capacitor is about 100 μm. For the sake of avoiding stray electric fields, the parallel plate capacitor is surrounded by guard rings [87]. The most remarkable characteristic in this capacitance dilatometer, however, is its high resolution ($\Delta l/l = 10^{-10}$), corresponding to absolute length changes of $\Delta l = 0.01$ Å for a specimen of length 10 mm. This resolution is roughly five orders of magnitude higher than that of conventional methods like neutrons or x-ray diffraction [73] and is mainly due to the high resolution of the capacitance bridge and the high quality of the plate capacitor in the dilatometer cell, which allows the detection of very small changes, i.e.changes of about 10^{-7} pF can be detected in the capacitance of the system. Two different high precision capacitance bridges have been used in these experiments: (a) Andeen Hagerling—Model 2500A 1 kHz and (b) General Radio—Model 1616. However, the above-mentioned resolution holds only until $T \simeq 40$ K, where a precise PID temperature control becomes difficult due to the large time constant involved in the experiment. As deduced in [87], the sensitivity of the measurements is proportional to the square of the starting capacitance (C^2). This means that the higher the starting capacitance, the higher the sensitivity. However, specimens of the molecular conductors investigated here are quite sensitive to the pressure applied by the dilatometric cell so that one cannot set a starting capacitance too high since this would consequently lead to a break in the sample. Hence, the starting capacitance for measurements under normal pressure (see Subsection 2.3) was limited to ∼18 pF. Just for completeness, it is worth mentioning that the empty capacitance of the system reads 16.7 pF.

For measurements under magnetic fields, a magnet power supply (model PS120-3) supplied by Oxford Instruments was used. In all performed measurements under magnetic fields reported here the field was applied parallel to the measured direction. For the direction-dependent thermal expansion measurements, the alignment of the crystal orientation was made using an optical microscope and guaranteed with an error margin of ±5°. To obtain the intrinsic thermal expansivity of the investigated specimen the thermal expansivity of copper of the dilatometric cell body was subtracted from the raw data. Apart from that, no further treatments like splines or any other kind of mathematical fittings were done.

The linear thermal expansion coefficient α_i in the direction i at constant P is defined as

$$\alpha_i = \frac{1}{l}\left(\frac{\partial l(T)}{\partial T}\right)_P, \tag{1}$$

where l refers to the sample length. The physical quantity described by equation (1) will be frequently used in this work. From the length changes of the sample $\Delta l(T) = l(T) - l(T_0)$ (T_0 is a fixed temperature), which is the physical quantity measured, the linear thermal expansion coefficient [equation (1)] was approximated by the differential quotient as

$$\alpha(T) \approx \frac{\Delta l(T_2) - \Delta l(T_1)}{l(300\,\mathrm{K}) \times (T_2 - T_1)}, \tag{2}$$

where $T = (T_1 + T_2)/2$ and T_1 and T_2 are two subsequent temperatures of data collection. Unless otherwise stated, in order to guarantee thermal equilibrium in all thermal expansion measurements reported here, a very low temperature sweep rate (± 1.5 K h^{-1}) was employed.

2.3. Thermal expansion measurements under quasi-uniaxial pressure

One of the challenges in the context of thermodynamic measurements is the realization of high-resolution thermal

expansion measurements under hydrostatic pressures, see e.g. [88].

However, by changing the starting capacitance and taking into account the contact area between the dilatometer and the sample, one can perform quasi-uniaxial thermal expansion experiments under pressures up to ∼100 bar employing the above-described setup, see e.g. [89]. The term 'quasi-uniaxial' is used here in the sense that one may have a pressure-gradient on the sample volume. The dependence between the force (F) exerted by the springs and the capacitance change (ΔC) can be easily measured and is given by

$$\frac{\Delta F}{\Delta C} = 0.124 \cdot \frac{\mathrm{N}}{\mathrm{pF}} \tag{3}$$

Making use of equation (3), the pressure applied by the dilatometric cell on the sample can be estimated. For example, taking a contact area of 0.2×10^{-6} m^2 and a capacitance change of 2 pF and using the definition of pressure $P = F/A$ results in a quasi-uniaxial pressure P of roughly 12 bar.

Hence, a slight change of the contact area and/or starting capacitance results in a significant change of the pressure exerted by the dilatometer on the sample. The crucial point of such experiments lies in the assembling and disassembling of the sample holder from the cryostat without damaging the sample, as such procedure is necessary to set the new starting capacitance (new pressure). As depicted in figure 11, for the (BEDT-TTF) based charge-transfer salts a hydrostatic pressure of a few hundred bar is enough to make a significant sweep across a wide range of the pressure-temperature phase diagram. Measurements under quasi-uniaxial pressure, to be discussed in section 3.4, will show that a quasi-uniaxial pressure of a few tenth of bar changes the shape of the thermal expansion coefficient curves dramatically, indicating therefore that the properties of this material are altered.

3. Thermal expansion measurements on fully deuterated salts of κ-(ET)$_2$Cu[N(CN)$_2$]Br ('κ-D8-Br')

As otherwise stated, in order to reduce cooling-speed dependent effects, the temperature was decreased by a rate of $\sim -3\,\mathrm{K\,h^{-1}}$ through the so-called glass-like transition around 80 K[7] in all experiments reported here. figure 16 depicts the linear thermal expansivity (upper part) along the in-plane a-axis for crystals #1 and #3 together with the out-of-plane (b-axis) electrical resistivity[8] $\rho_\perp$ (lower part) for crystal #1. As depicted in figure 16, upon cooling, $\rho_\perp$ achieves a broad maximum centered at ∼45 K, then abruptly drops and levels out at ∼30 K. The electrical resistivity remains metallic, i.e. $\mathrm{d}R/\mathrm{d}T > 0$, down to ∼20 K, below which $\rho_\perp$ increases again (see upper inset in figure 16), indicating a phase transition to an insulating state. A comparable $\rho_\perp$ behavior was observed for the single crystal #3 as well as for the crystal investigated in [43], except for small differences around the maximum and some details in the insulating

[7] This cooling speed (∼−3 K h^{-1}) was employed in the temperature range ∼85–65 K. From room temperature down to ∼85 K as well as from 65 K down to 4.2 K, an average cooling speed of −40 K h^{-1} was employed.

[8] Resistance measurements shown in figure 20 were carried out by Strack.

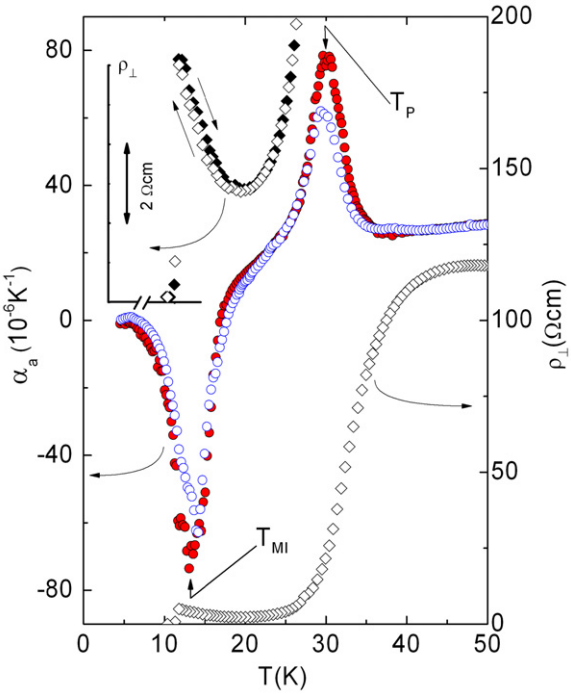

Figure 16. Left scale: thermal expansion coefficient along the in-plane a-axis, $\alpha_a(T)$, for crystals #1 (red) and #2 (blue); right scale: out-of-plane electrical resistivity, $\rho_\perp$, for crystal #1 of the κ-D8-Br salt. The upper inset depicts a zoom of the low temperature $\rho_\perp(T)$ data employing the temperature scale depicted in the main panel. Figure taken from [2].

regime. Interestingly enough, for all three crystals studied, $\rho_\perp$ vanishes below ∼11.5 K. A zero electrical resistivity followed by a very small feature in the thermal expansivity $\alpha_i(T)$ suggests percolative superconductivity coexisting with an antiferromagnetic insulating phase for κ-D8-Br [61], see the phase diagram presented in figure 8. In [1], Kawamoto *et al* performed a.c. magnetic susceptibility measurements on κ-D8-Br under two distinct conditions: (a) cooling the system slowly, namely employing a cooling-rate of 0.2 K min^{-1}; and (b) using a high cooling-rate of 100 K min^{-1}. From the measurements carried out after slow cooling, below the onset of superconductivity at $T_c = 11.5$ K, they did not observe a jump in the real part of the a.c. magnetic susceptibility, as expected for bulk superconductivity, but a gradual transition towards low temperatures. From the latter behavior they estimated a percolative superconducting volume fraction of 20% . In the case of measurements after rapid cooling, according to the authors, the superconducting volume fraction is reduced to 1–2%.

As can be seen in figure 16, some features observed in the electrical resistivity manifest themselves in the coefficient of thermal expansion as well. Indeed, the rather abrupt drop of $\rho_\perp$ is accompanied by a pronounced maximum in $\alpha_a(T)$ centered at a temperature $T_p \simeq 30$ K. As will be discussed in more detail below, this behavior can be assigned to a crossover phenomenon in the vicinity of a nearby critical point. Upon cooling the system further, $\alpha(T)$ reveals a huge negative peak, indicating a phase transition, see the phase diagram depicted in figure 8. The concomitant change in $\rho_\perp$ from metallic to

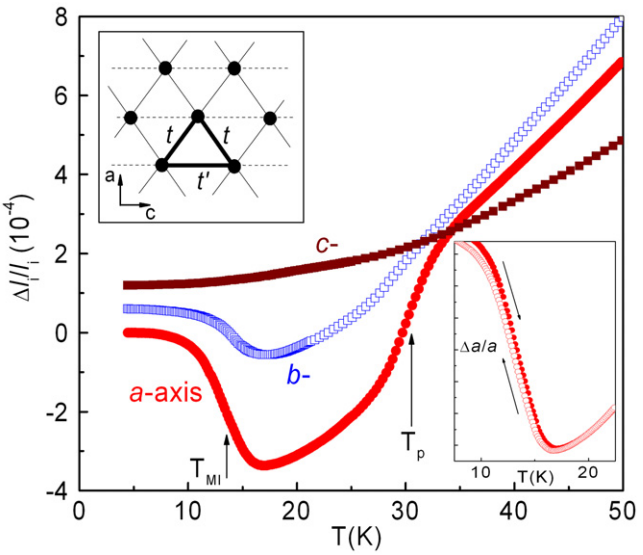

Figure 17. Main panel: relative length changes data $\Delta l_i(T)/l_i$, with $i = a, b, c$ for crystal #1 of the κ-D8-Br salt along the in-plane a- and c- and out-of-plane b-axis. For clarity, the data set have been offset. Lower inset: hysteresis in $\Delta l_a(T)/l_a$ associated with the Mott MI transition, measured under a very low temperature sweep-rate of $\pm 1.5\,\mathrm{K\,h^{-1}}$. Upper inset: 2D triangular-lattice dimer model with hopping terms t and t', the dots represent dimers of ET molecules. Figure taken from [2].

insulating behavior indicates that the peak in the expansivity data, $\alpha_a(T)$, is due to the Mott MI transition[9]. Note that a similar behavior of $\alpha_a(T)$ is observed for crystal #2, albeit with somewhat reduced (∼20%) peak anomalies at T_p and T_{MI}. This reduction might be related to small misalignments of the crystal as well as to different pressures exerted by the dilatometer cell on the crystals, approximately 4 bar for crystal #1 and 6 bar for crystal #2. More information on the nature of such transitions can be obtained via investigation of possible anisotropic lattice effects, namely by measuring and analysing the relative length changes along the three crystallographic directions, i.e. $\Delta l_i(T)/l_i = (l_i(T) - l_i(0\,\mathrm{K}))/l_i(300\,\mathrm{K})$ (with $i = a, b, c$), as depicted in figure 17.

As can be seen in figure 17, the most pronounced effects appear along the a-axis (in-plane), i.e. parallel to the polymeric ($Cu[N(CN)_2]Br$) anion chains, see figure 5. Of special interest is the 'S-shaped' anomaly near T_p which corresponds to the peak at T_p in $\alpha_a(T)$ (see figure 16) and does not show any trace of hysteresis upon cooling or warming, at least within the resolution of the present experiments. This is a generic feature of strong fluctuations in the vicinity of a critical end point. Upon further cooling through T_{MI}, the length of the crystal along the a-axis shows a distinct increase of roughly $\Delta l_a/l_a = 3.5{\cdot}10^{-4}$ within a very limited T-window, consistent with a broadened first-order phase transition. The assumption of a first-order phase transition is also supported by the observation of a hysteresis around T_{MI} of ∼0.4 K, as depicted in the lower inset of figure 17, which nicely agrees with the hysteresis observed in $\rho_\perp(T)$ (see upper inset of figure 16). The associated anomalies observed along the b-axis (out-of-plane) are clearly less pronounced. Notably, for the second in-plane direction (c-axis), anomalous behavior in $\Delta l_c/l_c$ can neither be detected at T_{MI} nor at T_p. The reliability of the previous results is supported by the same anisotropy observed for crystal #3, investigated in [43]. Based on the quasi-2D electronic structure of the present material, the observed anisotropic lattice effects at the Mott MI transition are very intriguing and deserve to be analyzed in more detail. The pronounced effects observed in the expansivity data along the in-plane a-axis, along which dimer–dimer overlap is absent, agree with the hypothesis that the diagonal hopping transfer integrals, t, play a crucial role in this process. Considering that these transfer integrals carry a net component along the in-plane c-axis, which is expected to be softer than the out-of-plane b-axis and second in-plane a-axis, a noticeable effect along the c-axis would then be naturally expected at T_{MI}. According to the authors of [94], the uniaxial isothermal compressibilities $k_i = l_i^{-1}(\mathrm{d}l_i/\mathrm{d}P)$ for the superconducting compound κ-$(ET)_2Cu(NCS)_2$ are robustly anisotropic with $k_1{:}k_2{:}k_3 = 1{:}0.53{:}0.17$ (ratio estimated under 1 bar), where k_1 refers to the isothermal compressibility along the in-plane c direction, k_2 along the second in-plane b-axis and k_3 along the direction parallel to a projection of the long axis of the ET donor molecules, i.e. along the out-of-plane a-axis for this salt, since its crystallographic structure is monoclinic [95]. Note that along the c-axis a direct dimer–dimer interaction t', as indicated in the upper inset of figure 17, exists, making a zero-effect along this axis even more surprising. A possible explanation for this feature would be a cancellation of counteracting effects related to the transfer integrals t and t', which seems to be improbable. Furthermore, it is not clear how these in-plane interactions may produce comparatively strong effects in the out-of-plane b-axis.

These findings provide strong evidence that other degrees of freedom, namely the lattice, should be somehow coupled to the π electrons, thus indicating that the Mott MI transition in the present material cannot be completely understood solely by taking into account a purely 2D electronic scenario [2].

3.1. Anisotropic lattice effects in κ-D8-Br and rigid-unit modes

In figure 18[10] the relative length changes in the T-range 4.2 K $< T <$ 200 K for the a-, b- and c-axes are shown. In the following, a possible explanation for the unusual anisotropic lattice effects observed in κ-D8-Br is presented.

Upon cooling, strongly anisotropic effects are observed in the whole temperature range. The more pronounced effects are observed along the in-plane a-axis, which is marked by a minimum around 150 K and an abrupt change in slope at T_g. This feature will be discussed in more detail below.

[9] In employing $\alpha = -80{\cdot}10^{-6}\,\mathrm{K^{-1}}$, obtained from the height of the anomaly in the thermal expansion coefficient for crystal #1 (figure 16), using the entropy change $\Delta S = -0.074\,\mathrm{J\,mol^{-1}\,K^{-1}}$ at the Mott MI transition, whose detailed deduction is presented in section 3.2, results in a jump of the specific heat of about $0.2\,\mathrm{J\,mol^{-1}\,K^{-1}}$. Details of this estimate are provided in appendix 2. This value corresponds roughly to 0.4% of the background at T_{MI} in the specific heat (specific heat measurements on κ-D8-Br crystal #1 were performed by Köhler) employing ac calorimetric method, so that no signatures in the specific heat at T_{MI} could be detected.

[10] In [72] Grießhaber refers to a cooling rate of $\sim -1\,\mathrm{K\,min^{-1}}$ as a slow cooling, while the rapid cooling rate is not mentioned.

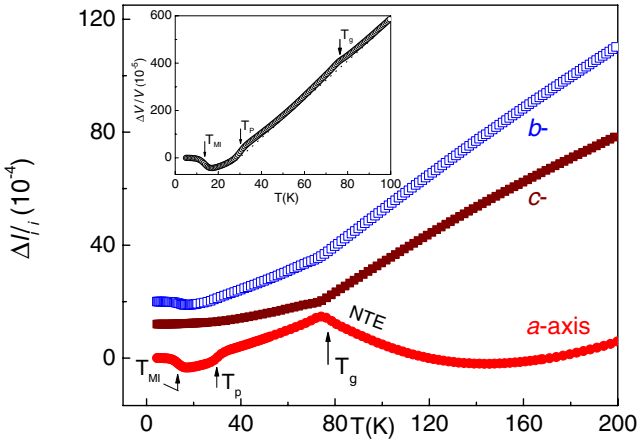

Figure 18. Main panel: relative length changes along the a- and c-axis (in-plane) and b-axis (out-of-plane) for κ-D8-Br crystal #1 up to 200 K. Data along the b- and c-axes are shifted for clarity. Position of T_g estimated according to [25]. NTE indicates negative thermal expansion along the a-axis (in-plane) in the T-range $T_g < T \lesssim 150$ K. Inset: relative volume change $\Delta V/V = \Delta l_a/l_a + \Delta l_b/l_b + \Delta l_c/l_c$ versus T. Low temperature data will be used for estimating the entropy change associated with the Mott MI transition (section 3.2). Figure after [3].

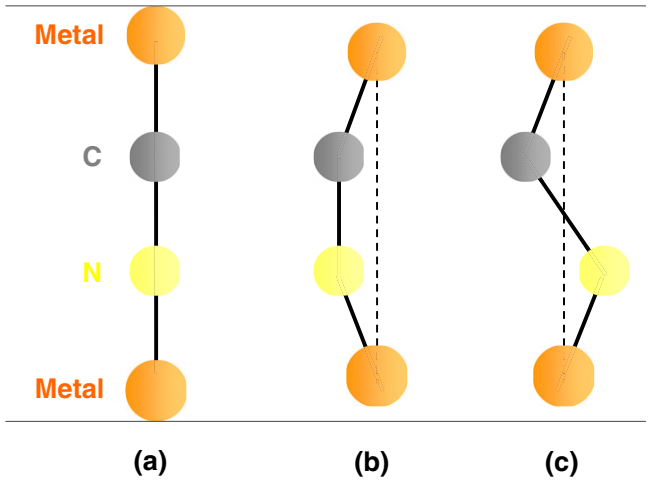

Figure 19. Schematic representation of the M-CN-M linkage. (a) Linear configuration. (b) Shift of the carbon (C) and nitrogen (N) atoms aside from the metal–metal axis in the same direction. (c) Shift in the opposite direction. Note that the total length along the metal–metal axis is reduced due to the displacement of the C-N atoms. This is a mechanism giving rise to negative thermal expansion. Figure reproduced after [99].

An interpretation in terms of disorder due to the freezing-out of the ethylene groups of the ET molecules either in the staggered or in the eclipsed configuration was proposed by Müller *et al* [25]. By substituting the terminal $(CH_2)_2$ groups by $(CD_2)_2$, one observes a shift of T_g to higher temperatures. A feature that is expected because of the higher mass of the $(CD_2)_2$ in comparison to the mass of the $(CH_2)_2$ groups, which in turn implies a higher relaxation time at a given temperature. Hence, the model proposed by Müller *et al* is supported by the so-called isotope effect. However, it does not explain the negative expansivity along the a-axis (in-plane) observed above T_g, namely in the interval $T_g < T \lesssim 150$ K. More recently, high-resolution synchrotron x-ray diffraction experiments [97] have provided indications that such an anomaly is not solely linked to the ethylene groups freezing-out. Essentially, the claims of the authors are based on the comparison between the estimated number of the disordered ethylene groups (staggered configuration) at 100 K (∼11%) with those at extrapolated zero temperature ($3 \pm 3\%$). They conclude that such a transition is most likely related to structural changes, probably involving the insulating polymeric anion chains. Upon further cooling, the anomalies at T_p and T_{MI}, already discussed in detail in the previous section, show up. From figure 18 it becomes clear that the lattice effects at T_g, T_p and T_{MI} are more pronounced along the polymeric anion chain a-axis, with negative thermal expansion (NTE), i.e. a decrease of length with increasing temperature, observed below T_{MI} (due to charge carrier localization) and also in the temperature window $T_g < T \lesssim 150$ K. It should be noted that the in-plane anisotropy at both T_{MI} and T_g corresponds to an orthorhombic distortion. Recently, NTE was also observed by Goodwin *et al* in other materials containing cyanide bridges in their structures, see [98, 99] and references therein. These authors proposed a simple model [99] to explain the origin of this unusual behavior. In this model, the transverse vibrational displacement of the CN units, away from the metal–metal axes (figures 19(b) and (c)), is assigned to be the mechanism responsible for NTE in these materials. As a matter of fact, NTE is also observable in other materials. For example, the NTE of liquid water below 4 °C is connected with a breaking of the tetrahedral H bonding. Below 4 °C, NTE is required to overcompensate the increase of entropy due to such a structural transition [101]. Another example can be found in ZrW_2O_8. This material exhibits NTE over a wide temperature window of 50–400 K [102]. The origin of this anomalous behavior is assigned to its structural arrangement, which is built up by WO_4 tetrahedra and rigid ZrO_6 octahedra. Rigid-unit modes in this material show up due to the fact that each WO_4 unit has one vertex not shared by another unit.

The displacement of the C and N atoms aside from the metal–metal axis has the effect of decreasing the distance between the metal atoms as the temperature is increased, see figures 19(b) and (c). According to the authors of [99], in polymeric crystalline materials, these vibrational modes will not occur separately, but rather they will affect the vibration modes of other metal-CN-metal linkages, giving rise to the NTE phenomenon. Nevertheless, the deformation of the metal-cyanide bridge will carry a high-energy penalty. Hence, assuming that the metal coordination geometries are preserved, the vibration modes illustrated in figures 19(b) and (c) can be observed only if they are coupled with the crystal lattice in the form of phonon modes. Yet, according to Goodwin *et al* such modes are referred to as rigid-unit modes (RUM) and can be experimentally observed in the low-energy window 0–2 THz, i.e. in the range of typical phonon frequencies [103]. Since the $Cu[N(CN)_2]Br^-$ (figure 5) counter anion has a polymeric nature, the above-described model is a good candidate to explain why NTE is observed only along the in-plane anion chain a-axis. The latter might have their origin in the RUM of dicyanamide $[(NC)N(CN)]^-$ ligands along the anion

polymeric chain. Note that the contraction of the lattice with growing T above T_g along the a-axis is accompanied by an expansion along the b- and c-axes. In addition, preliminary Raman studies (not shown here), carried out on κ-D8-Br (crystal #4), revealed the appearance of a double peak structure in the frequency window 50–200 cm^{-1} at 20 K (below T_g), not observed at 130 K (above T_g, but below the onset of NTE) [100]. Further systematic studies are required to verify if such splitting shows up above or below T_p. Note that this frequency window fits roughly into the above-mentioned energy window predicted for RUM. Interestingly enough, the double peak structure is not observed at 5 K (below T_{MI}), indicating that vibration modes in this energy window are no longer active below T_{MI}. Hence, these results support the idea of strong coupling between lattice and electronic degrees of freedom at the Mott transition. Still owing to the anomalous lattice effects above T_g, based on the above discussion, it seems that the freezing-out of the degrees of freedom of the ethylene end-groups of the ET molecules in the staggered/eclipsed configuration alone cannot be responsible for a NTE along the a-axis. Indeed, as pointed out in [104], the glass-like anomaly is not observed in the organic superconductors β''-$(ET)_2SF_5CH_2CF_2SO_3$ ($T_c = 5$ K, large discrete anion) and in κ-$(ET)_2I_3$ ($T_c = 3.5$ K, linear anion) as well as in the nonsuperconducting α-$(ET)_2KHg(SCN)_4$ (polymeric anion). For such materials, a smooth Debye-like behavior along the three crystallographic directions up to 200 K is observed, i.e. no glass-like transition is observed. It is appropriate to mention here that the glass-like anomaly is not observed in the κ-$(ET)_2Cu_2(CN)_3$ salt, to be discussed in section 5. Thus, a possible scenario to explain this feature for the κ-$(ET)_2Cu[N(CN)_2]Z$ salts would be the existence of a complicated entwinement between the ethylene end groups and the vibration modes of the polymeric anion chain, not knowingly reported as yet in the literature. According to this idea, the ethylene end groups delimit cavities, where the anions are trapped [34], so that below T_g an anion ordering transition occurs in a similar way to the anion ordering transition observed in the quasi-1D $(TMTCF)_2X$ charge-transfer salts [105]. Further systematic Raman and infra-red studies are necessary to provide more information about the nature of the glass-like transition.

3.2. Entropy change associated with the Mott MI transition

More information about the Mott physics in the present materials can be obtained by estimating the amount of entropy linked to the Mott MI transition. Such entropy change is directly associated with the slope of the first-order phase transition line in the *universal* P-T phase diagram figure 8 and the volume change associated with the Mott MI transition by the Clausius–Clapeyron equation, which reads

$$\frac{\mathrm{d}T_c}{\mathrm{d}P} = \frac{\Delta V}{\Delta S}. \tag{4}$$

Here, $\Delta V = (V_I - V_M)$ ($\Delta S = (S_I - S_M)$) refer to the difference in volume (entropy) between the insulating (I) and metallic (M) states. Employing $\mathrm{d}T_{\mathrm{MI}}/\mathrm{d}P = (-2.7 \pm 0.1)\,\mathrm{K\,MPa}^{-1}$, as obtained from the slope of the S-shaped line at T_{MI} in figure 8 and $\Delta V/V = (4.2 \pm 0.5) \times 10^{-4}$, as estimated from the inset of figure 18, one obtains $\Delta S = -0.074\,\mathrm{J\,mol}^{-1}\,\mathrm{K}^{-1}$. This small entropy change at T_{MI} represents a subtle fraction of the full entropy related to the metallic state of the κ-H8-Br salt at $T \simeq 14$ K of $S = \gamma \cdot T \simeq 0.375\,\mathrm{J\,mol}^{-1}\,\mathrm{K}^{-1}$, using the Sommerfeld coefficient $\gamma = 0.025\,\mathrm{J\,mol}^{-1}\,\mathrm{K}^{-2}$ [106]. Electronic specific heat data by Nakazawa *et al* [107] revealed that by means of gradual deuteration it is possible to tune the system from the Mott insulating state to the metallic regime of the phase diagram. As observed in these experiments, γ decreases towards zero in the insulating phase. Based on these literature results, γ of the fully deuterated salt discussed in this work should actually be somewhat smaller than that of the fully hydrogenated salt. It follows that the small entropy change of $-0.074\,\mathrm{J\,mol}^{-1}\,\mathrm{K}^{-1}$, estimated as above-described, demonstrates that the spin entropy of the paramagnetic insulating state at elevated T must be almost completely removed. In addition, this result is consistent with the Néel temperature T_N coinciding with T_{MI} at this point in the phase diagram [108].

3.3. Magnetic field effects on κ-D8-Br

Having detected unusual features in the thermal expansivity of κ-D8-Br, additional information about the role played by lattice degrees of freedom for the Mott MI transition in κ-D8-Br can be obtained by carrying out thermal expansion measurements under magnetic fields. In what follows we discuss the effects of magnetic fields in the expansivity data at the immediate vicinity of the Mott transition. However, before doing so, let us consider first the low-temperature case at zero magnetic fields. The thermal expansivity along the b-axis (out-of-plane) for $B = 0$ is shown in figure 20 together with the electrical resistance[11] data normalized to its value at room temperature. Upon cooling, a negative anomaly in the expansivity data at around $T = 13.6$ K is observed. The latter is linked to the Mott MI transition and mimics the lattice response upon crossing the first-order Mott MI transition line in the phase diagram, see the discussion in the previous sections. Note that the anomaly in $\alpha_b(T)$ is directly connected to an enhancement of the electrical resistance around the same temperature, which corroborates the assumption that the anomaly in the expansivity $\alpha_b(T)$ is triggered by the Mott MI transition. The drop of the electrical resistance at $T_c = 11.6$ K, accompanied by a very small kink (indicated by an arrow) in $\alpha_b(T)$, are fingerprints of percolative SC in small portions of the sample volume coexisting with the AF ordered insulating state, see e.g. [109]. In the temperature window 12 K $\lesssim T \lesssim$ 16 K, jumps in the electrical resistance are noticeable. In fact, such jumps in $R(T)$ are frequently observed in organic charge-transfer salts. The huge expansivity of the crystal, which in turn is due to the softness of this class of materials, induces stress on the electrical contacts, giving rise to such jumps. In general, the appearance of jumps in resistivity data are attributed to cracks in the crystal. For the quasi one-dimensional $(TMTTF)_2X$ and $(TMTSF)_2X$ salts, in particular,

[11] See footnote 8.

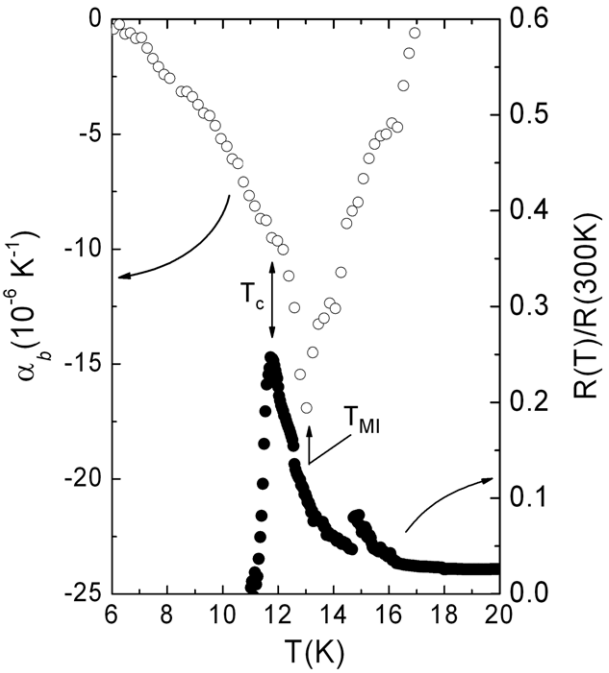

Figure 20. Left scale: thermal expansion coefficient along the out-of-plane b-axis. Right scale: electrical resistance data normalized to its value at room temperature, being both data set for κ-D8-Br crystal #3. T_{MI} denotes to the Mott MI transition temperature and T_c refers to the percolative SC critical temperature. Jumps in the resistance around 13 K and 15 K are most likely related to the large expansivity of the material in this temperature range, as discussed in the text. Figure taken from [3].

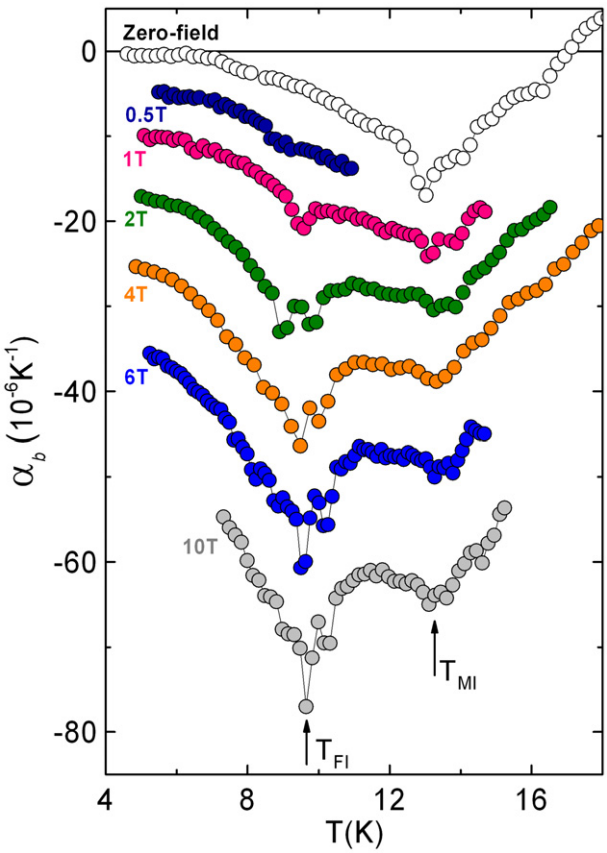

Figure 21. Thermal expansion coefficient perpendicular to the conducting layers under selected fields for the κ-D8-Br crystal #3. T_{MI} refers to the Mott MI transition temperature and T_{FI} to the field-induced phase transition temperature, as discussed in the main text. Figure reproduced after [85].

such jumps in the resistivity data are assigned to stress caused by localized defects and/or to mechanical twinning [12].

The thermal expansivity data along the b-axis (out-of-plane) at low-T under external magnetic fields of 0, 0.5, 1, 2, 4, 6 and 10 T [85] is depicted in figure 21. From this data one can directly see that upon reducing T under a magnetic field up to 10 T, the Mott MI transition temperature T_{MI} stands essentially unaffected. Nevertheless, upon reducing T further under a low magnetic field of 0.5 T, a second *field-induced* anomaly at around $T_{FI} = 9.5$ K is observed. Increasing the magnetic field, this anomaly becomes more and more pronounced, until it saturates at around ∼4 T. A careful analysis of the data shown in figure 21 reveals the presence of a double-peak structure for magnetic fields higher than 1 T. However, further experiments are necessary to gain more insights into this feature. No such magnetic field-induced effects were observed along the in-plane a- and c-axis (not shown). As known from the literature, see e.g. [110], orientational field-dependent magnetic phenomena may indicate a spin-flop (SF) transition. Such a transition takes place when the system is in an AFI state and a magnetic field, exceeding a certain critical value (critical field), is applied parallel to the so-called easy-axis. In the present case, this field dependence of the thermal expansivity $\alpha_b(T)$ is suggestive of a SF transition with strong magneto-elastic coupling. As can be directly seen from figure 21, the magnetic critical field H_c is smaller than 0.5 T for κ-D8-Br, which is consistent with $H_c \sim 0.4$ T for the κ-(ET)$_2$Cu[N(CN)$_2$]Cl salt, as obtained by Miyagawa *et al.* in [56]. The physical explanation why the anomaly in the expansivity $\alpha_b(T)$ at $T = T_{FI}$ becomes more evident for magnetic fields higher than H_c, however, cannot be based solely in terms of a SF transition, so that a possibly different mechanism might be related to this feature. It was pointed out by Ramirez *et al* in [111] that the emergence of pronounced anomalies under finite magnetic fields in thermodynamic quantities, like the specific heat or thermal expansion, have only been observed in a few systems and can be considered as unusual physical phenomena. Let us discuss two possible distinct scenarios to explain this unusual feature:

(i) First of all, electrical resistance measurements carried out on partially deuterated κ-(ET)$_2$Cu[N(CN)$_2$]Br salts under magnetic field sweeps, being the magnetic field applied along the out-of-plane b-axis and the temperature fixed at $T = 5.50$ K and 4.15 K for 50% and 75% salts, respectively, unveiled a sudden change from SC to high resistive-states for magnetic fields of about 1 T [85, 112]. Such a state was found to transform into a high-resistive state via jump-like increases in the electrical resistance upon further increasing the applied magnetic field to 10 T [112]. The authors of [112] interpreted this behavior as a magnetic field-induced first-order SC-to-Insulator transition and related it to the theoretical description

based on the SO(5) symmetry for superconductivity and antiferromagnetism, as proposed for the high-T_c cuprates by Zhang [113]. Moreover, upon tuning the κ-$(ET)_2Cu[N(CN)_2]Cl$ salt close to the Mott MI transition by hydrostatic pressure [44] a pronounced B-induced increase in the electrical resistance was observed also for this salt. In the latter case, it was proposed that minor metallic/superconducting phases near the Mott MI transition undergo a magnetic field-induced localization transition see theoretical predictions, see, e.g. [114] and references cited therein. Thus, based on these findings, it is natural to expect that also for the fully deuterated κ-$(ET)_2Cu[N(CN)_2]Br$ salt, located on the verge of the Mott MI transition line in the phase diagram, the electronic states may undergo drastic changes upon increasing the strength of the applied magnetic field. Based on the above discussion, the growth of the anomaly in $\alpha_b(T)$ with increasing fields $H > H_c$ may be related with the sensitivity of the electronic channel to applied magnetic fields in this particular region of the phase diagram. In fact, the initial rapid growth and the tendency to saturation for field above about 4 T is quite similar to the evolution of the electrical resistance, i.e. the increase of $R(B, T = \text{const.})$ with field observed in the above-mentioned transport studies [44, 112]. It is worth mentioning that no such magnetic field-induced effects were observed for fields applied parallel to the in-plane a- and c-axis (not shown), supporting thus the hypothesis of a SF transition. Indeed, it was pointed out in [115] that the type of the inter-layer magnetic ordering strongly depends on the direction of the applied magnetic field. In particular, based on a detailed analysis of NMR and magnetization data, taking into account the Dzyaloshinskii–Moriya interaction, the atuhors of [44, 112] found that inter-plane antiferromagnetic ordering can be observed *only* for magnetic fields exceeding H_c applied along the out-of-plane b-axis. We stress that the term *'inter-plane afm ordering'* is used here as defined in figures 4 and 5 of [115]. Thus, given the absence of lattice effects at T_{FI} for magnetic fields applied along the in-plane a- and c-axis, the present results suggest a close relation between inter-plane antiferromagnetic ordering and the lattice response observed at T_{FI}. Employing the same notation used by the authors of [115], the magnetization of the $+(-)$ sublattice at the layer l is $\mathbf{M}_{+(-)l}$., being the staggered and ferromagnetic moments given by $\mathbf{M}_l^{\dagger} = (\mathbf{M}_{+l} - \mathbf{M}_{-l})/2$ and $\mathbf{M}_l^{F} = (\mathbf{M}_{+l} + \mathbf{M}_{-l})/2$, respectively. For fields above H_c applied along the out-of-plane b-axis, $\mathbf{M}_l^{F}$ is along the b-axis and $\mathbf{M}_l^{\dagger}$ lies in the a-c plane. $\mathbf{M}_A^{\dagger}$ and $\mathbf{M}_B^{\dagger}$ are antiparallel, giving rise to an inter-plane antiferromagnetic ordering. The pronounced negative peak anomaly in $\alpha_b(T)$ observed at $T = T_{FI}$ suggests that in order to obtain this particular spin configuration, the increase in exchange energy forces the $(ET)_2^+$ layers to move apart from each other.

(ii) A possible second interpretation for the sharp peaks in $\alpha_b(T)$ induced by a magnetic field is that upon exceeding the critical field H_c, percolative superconductivity is destroyed, the remaining electron spins do not couple with the applied magnetic field due to the correlated motion among them. These field-decoupled spins are strongly coupled to the lattice and give rise to the minimum at T_{FI}. The term field-decoupled spins is used in [111] to refer to a similar effect (double peak structure) observed in specific heat measurements under magnetic field for the 'spin ice' compound $Dy_2Ti_2O_7$. According to the authors of [111], for magnetic fields applied parallel to the [1 0 0] crystallographic direction, due to correlated motion among the spins, half the spins have their Ising-axis orientated perpendicular to the magnetic field. The latter are called decoupled-field spins. It was observed that magnetic fields exceeding a certain critical value lead to the ordering of these field-decoupled spins. Monte Carlo calculations, also reported by the authors in [111], support the proposed model. The term 'spin ice' is used by the authors to refer to the spin orientations in analogy with the degeneracy of ground states observed in ice (H_2O in solid phase), where hydrogen atoms are highly disordered and give rise to a finite entropy as $T \to 0$. This is because the oxygen atoms in water form a well defined structure, while the hydrogen atoms remain disordered as a result of the two inequivalent O-H bond lengths, as first pointed by Pauling [116]. The present results do not enable us to determine the exact orientation of these field-decoupled spins.

It is worth mentioning that the above-discussed scenarios should be seen as 'possible scenarios' and that the concrete physical origin of the features observed at T_{FI} remain elusive. Another particularity in the data presented in figure 21 is that for magnetic fields $H > H_c$, in a temperature range between T_{MI} and T_{FI}, an intermediary phase appears, probably paramagnetic, as depicted in the schematic phase diagram in figure 22. It is tempting to speculate that this feature can be seen as a separation of the T_N and T_{MI} lines in the phase diagram. A possible physical description to this would be related to the energetic competition between the AFI ordered phase and the paramagnetic phases after crossing the MI first-order line, resulting thus in a decrease of T_N with increasing magnetic field. Similar experiments were performed in two other κ-D8-Br crystals (crystals #1 and #2). However, for both crystals, in contrast to the pronounced anomaly observed at $T_{FI} \approx 9.5$ K under magnetic fields (figure 21), the application of magnetic fields results in a smooth change of the out-of-plane expansivity $\alpha_b(T)$ around the same temperature. In this regard, two factors should be considered as a possible explanation for the absence of the above-described effects:

(i) As described in e.g. [117], the SF transitions are very sensitive to the alignment between the applied magnetic field and the easy-axis. A subtle misalignment between the magnetic field and the easy-axis can therefore give rise to a suppression of the transition;

(ii) The absence of a sharp transition can also be due to sample inhomogeneities and defects. Sample inhomogeneities would imply, for instance, that portions of percolative SC may vary from sample to sample, reflecting therefore differences in their magnetic properties [1].

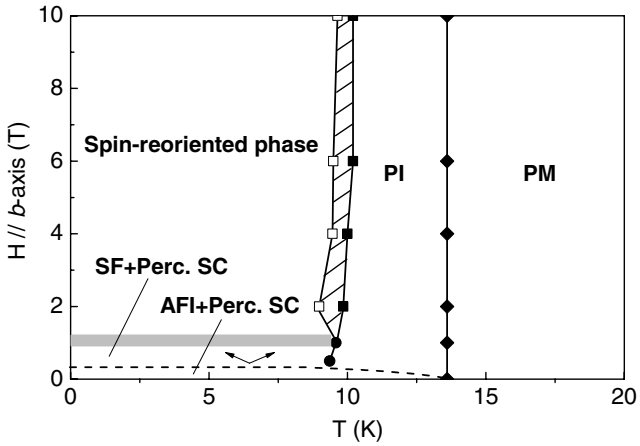

Figure 22. Schematic H-T diagram for κ-D8-Br for a magnetic field applied along the out-of-plane b-axis. Symbols indicate the peak anomaly observed in the expansivity $\alpha_b(T)$, while lines refer to the various phase transitions, see the discussion in the main text. PI and PM stand, respectively, for the paramagnetic insulator and the paramagnetic metal. The hatched area marks the temperature interval in which a double-peak structure in $\alpha_b(T)$ is observed. Spin-reoriented phase denotes the region where $\mathbf{M}_A^{\dagger}$ and $\mathbf{M}_B^{\dagger}$ are antiparallel, giving way to an inter-plane antiferromagnetic ordering, see the discussion in the main text. Figure reproduced after [3, 85].

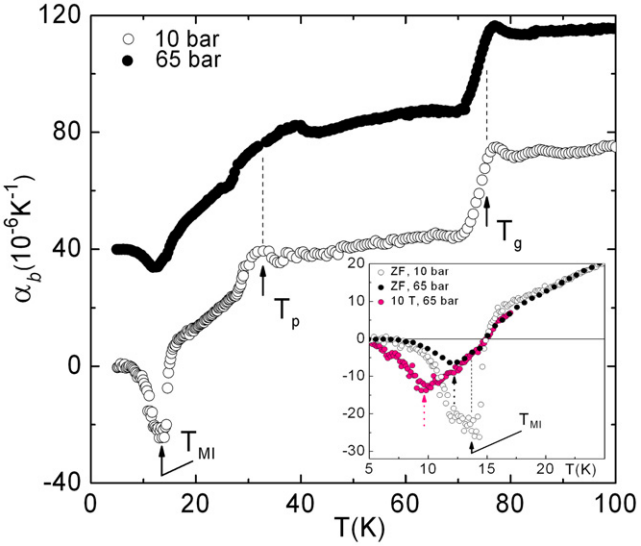

Figure 23. Main panel: thermal expansion coefficient along the out-of-plane b-axis for κ-D8-Br crystal #2 under ambient (10 bar) and quasi-uniaxial pressure of 65 bar. Dashed lines are guide for the eyes. For clarity, data are shifted. Inset: blowup of the low-T $\alpha_b(T)$ data together with measurement under pressure (65 bar) and magnetic field of 10 T. ZF refers to zero magnetic field. The black dashed arrow indicates the peak position under quasi-uniaxial pressure of 65 bar, while the pink dashed arrow highlights a shift of the peak position to lower T when a magnetic field of 10 T is applied. Figure after [3].

The present findings are compiled in the schematic T versus H diagram shown in figure 22. The dashed line around $\sim$0.5 T defines the separation boundary between the AFI and the SF phases. The thick line indicates the suppression of percolative SC giving place to field-decoupled and/or flopped spins, here referred to as mixed states.

Concluding this section, the thermal expansion results on κ-D8-Br along the out-of-plane b-axis under a magnetic field show that the Mott MI transition in this salt is largely field-independent under magnetic fields up to at least 10 T. Such findings are consistent with the picture of a Mott insulator formed by a set of hole localized in dimers formed by two ET molecules [22]. At $T_{\rm FI} = 9.5$ K a phase transition induced by a magnetic field is observed, indicative of a SF transition with strong magneto-elastic coupling, accompanied by an enhancement of $\alpha_b(T)$ due to the suppression of the percolative SC under magnetic fields above 1 T. Further experiments, like magnetostriction measurements above and below $T_{\rm FI}$ are highly desired to shed more light on the above-discussed magnetic field-induced lattice effects.

3.4. Thermal expansion under quasi-uniaxial pressure

Given the high anisotropy of the κ-$(ET)_2X$ charge-transfer salts, thermal expansion measurements under quasi-uniaxial pressure could provide more insights to better understand the transitions at $T_{\rm MI}$, T_p and T_g. The effect of quasi-uniaxial pressure on the sample was studied for crystal #2 as shown in figure 23. In these experiments, a pressure of (65 ± 5) bar was applied along the out-of-plane b-axis. Roughly speaking, pressure application along the b-axis means a change of the contact between the polymeric-anion chains and the ET molecules and/or enhancement of the tilt of the ET molecules.

As shown in the main panel of figure 23, the shape of the expansivity curves at $T_{\rm MI}$ and T_p is dramatically changed by applying a quasi-uniaxial pressure of 65 bar. These findings reveal that the anomalies observed in the out-of-plane expansivity $\alpha_b(T)$ at $T_{\rm MI}$ and T_p are strongly affected upon applying pressure, while T_g remains practically unaffected. Since κ-D8-Br is located on the boundary of the Mott MI transition (figure 8), this feature might be associated with a slight shift of its position from the insulating to the metallic side of the phase diagram. Assuming the peak position $T_{\rm MI} = 13.6$ K as the transition temperature under ambient pressure (actually under a pressure of roughly 10 bar) and $T_{\rm MI} = 11.8$ K as the transition temperature under quasi-uniaxial pressure (65 bar), one obtains $\mathrm{d}T_{\rm MI}/\mathrm{d}P_b \simeq -33\,\mathrm{K\,kbar^{-1}}$. Such a value is roughly one order of magnitude smaller than the hydrostatic pressure dependence of $T_{\rm MI}$ ($\mathrm{d}T_{\rm MI}/\mathrm{d}P \simeq -380\,\mathrm{K\,kbar^{-1}}$), estimated from the slope of the Mott MI transition line in figure 8 at $T = 11.8$ K. Such discrepancy might reflect the anisotropy in the uniaxial-pressure effects. However, the shift of T_p ($T_{\rm MI}$) to high (low) temperatures is in perfect agreement with a positive (negative) pressure dependence of T_p ($T_{\rm MI}$) in the phase diagram (figure 8). Applying a magnetic field of 10 T (pink curve in the inset of figure 23), the peak position of the transition, indicated by black and pink dashed arrows, shifts to lower temperatures. As $T_{\rm MI}$ is insensitive to magnetic fields up to 10 T (section 3.3), this observation suggests that the anomaly in $\alpha_b(T)$ under quasi-uniaxial pressure should be triggered by superconductivity. The present thermal expansion results under quasi-uniaxial pressure can be seen as a starting point for experiments under hydrostatic pressure, which will

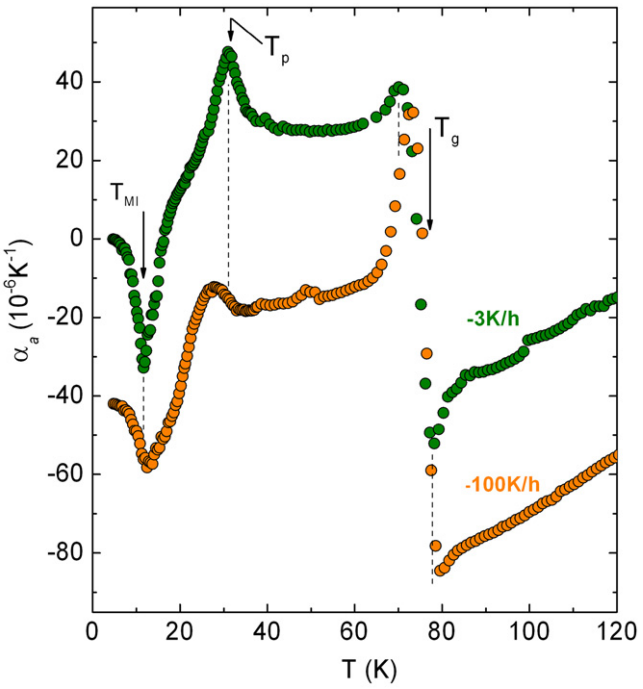

Figure 24. Thermal expansion coefficient as a function of temperature for κ-D8-Br crystal #3 along the in-plane a-axis. Measurements taken on warming after employing different cooling speeds ($-3\,\mathrm{K\,h^{-1}}$ and $-100\,\mathrm{K\,h^{-1}}$). Data are shifted for clarity. Arrows indicate the respective transition temperatures for the slowly cooled crystal. Dashed lines are used to show the shift of T_{MI} (towards higher temperatures), T_p (towards lower temperatures) and T_g (towards higher temperatures) under fast cooling across T_g. Figure after [3].

provide important information about the physics in the vicinity of the Mott MI transition region in the phase diagram.

3.5. Influence of the cooling speed on T_g in κ-D8-Br

In this section, the influence of the cooling speed below the glass-like transition at $T_g \approx 77\,\mathrm{K}$ on T_{MI} and T_p is discussed. In fact, the role of the cooling speed on the physical properties of fully and partially deuterated salts of κ-$(\mathrm{ET})_2\mathrm{Cu[N(CN)_2]Br}$ has been intensively discussed in the literature, see e.g. [109, 118]. As shown in figure 24, the expansivity along the in-plane a-axis for a crystal of κ-D8-Br was measured after cooling the sample through the so-called glass-like phase transition by employing two distinct cooling speeds ($-3\,\mathrm{K\,h^{-1}}$ and $-100\,\mathrm{K\,h^{-1}}$).

A broadening of the transition, accompanied by a reduction in the size of the peak anomaly at $T_p \simeq 30\,\mathrm{K}$, which is related to the critical end-point of the first-order Mott MI transition line in the phase diagram and the Mott MI temperature $T_{\mathrm{MI}} \simeq 13.6\,\mathrm{K}$, is observed for fast cooling ($-100\,\mathrm{K\,h^{-1}}$). Another remarkable feature is that the peak position of the $T_p = 30\,\mathrm{K}$ anomaly shifts toward lower temperatures, while the anomaly at $T_{\mathrm{MI}} = 13.6\,\mathrm{K}$ shifts slightly to higher temperatures. Based on these observations, one can conclude that the increase of the cooling speed through T_g results in an opposite effect to that observed upon applying quasi-uniaxial pressure (section 3.4). The observed shift of T_g towards higher temperatures under fast cooling is in agreement with literature results [25]. Resistivity measurements on κ-D8-Br salts [72, 119], synthesized by employing the same method as that used for the salts studied in this work, revealed that under a fast cooling speed[12] the resistance increases dramatically below $T_g \simeq 80\,\mathrm{K}$, superconductivity is suppressed, giving way to a residual resistance ratio of $\sim$5. This feature together with the observed enhancement of the anomaly in α_a on fast cooling (figure 24) can be assigned to an increase of the scattering provoked by the randomly distributed potential of the polymeric $\mathrm{Cu[N(CN)_2]Br^-}$ anion. A similar situation is encountered in the quasi-1D $(\mathrm{TMTSF})_2\mathrm{ClO_4}$ superconductor salt, where by rapid cooling ($>50\,\mathrm{K\,min^{-1}}$) superconductivity is destroyed, giving way to a first-order anion-ordering transition at $T = 24\,\mathrm{K}$, which is accompanied by a spin-density wave transition around 6 K [12].

4. Mott criticality

Before discussing the Mott criticality in detail, let us first present a general discussion about critical behavior and universality classes.

4.1. Critical behavior and universality classes

Continuous phase transitions involve fluctuations on all length scales, leading to the remarkable phenomenon called universality. While details of the interaction do not matter, only robust properties of the system like its effective dimensionality, the absence or presence of long-range interactions or the symmetry of relevant low-energy fluctuations determine the low-energy behavior. As a consequence, it is possible to classify continuous phase transitions according to their universality classes.

In real materials, upon approaching the critical temperature, fluctuations are no longer negligible. The more the critical temperature is approached, the stronger are the fluctuations. Finally, fluctuations succeed in destroying the original phase and a new phase, often with distinct symmetries, emerges. To distinguish the two different phases, one usually tries to introduce an order parameter as the expectation value of some field which vanishes in one phase but not the other.

The transition is, in many cases, accompanied by broadening effects due to crystal defects or inhomogeneities. Amazingly, around T_c some physical quantities tend to obey power laws in the reduced temperature $t = (T - T_c)/T_0$, which measures the relative distance to the transition temperature. As a consequence of universality, the divergence of the compressibility of water in the vicinity of its critical point is described by exactly the same power-law dependence as the divergence of the susceptibility of a uniaxial magnet in the vicinity of the Curie temperature. In such a uniaxial magnet, the spins can only align themselves parallel or anti-parallel to a given crystal axis. As the magnetization is finite in the symmetry-broken state below T_c and vanishes above T_c, the expectation value of the magnetization may serve as an order parameter.

[12] See footnote 10.

Concerning thermodynamic properties, one usually defines the four critical exponents $\tilde{\alpha}$, β, γ and δ, which in the case of magnets are related to the specific heat (at constant pressure) $C_p(T)$, the spontaneous magnetization $M_s(T)$ and the susceptibility $\chi(T)$. More generally, $M_s(T)$ and $\chi(T)$ describe the order parameter and the order parameter susceptibility. Usually, α is used in the literature to refer to the specific heat critical exponent. In order to avoid any confusion with the linear thermal expansion coefficient $\alpha(T)$, here, $\tilde{\alpha}$ is used to refer to the specific heat critical exponent.

Close to criticality, one expects the following power-law behavior,

$$C_p(T) \sim A^{\pm} \frac{|t|^{-\tilde{\alpha}}}{\tilde{\alpha}}, \tag{5}$$

$$M_s(T) \sim B|t|^{\beta}, t \leqslant 0, \tag{6}$$

$$\chi(T) \sim C^{\pm}|t|^{-\gamma}, \tag{7}$$

$$M_s(H) \sim DH^{1/\delta}, t = 0. \tag{8}$$

While the amplitudes $A^{\pm}$, B, $C^{\pm}$ and D are non-universal and the coefficients A^+ and C^+ governing the behavior for $t > 0$ are generally different from the corresponding coefficients A^- and C^- for $t < 0$, the ratios A^+/A^- and C^+/C^- are in fact universal, i.e. they are not material-specific and only depend on the underlying universality class. In fact, not all of the above exponents are independent. Using concepts of scaling or the renormalization group, the following identities can be derived [120–124],

$$\tilde{\alpha} + 2\beta + \gamma = 2, \tag{9}$$

$$\gamma = \beta(\delta - 1). \tag{10}$$

These two relations are frequently called the Rushbrooke and Widom identities. It is striking to note that in the study of critical behavior near a second-order phase transition, materials displaying completely different crystal structures as well as quite different subsystems obey the same critical behavior near T_c, giving thus rise to the universality classes. The theoretical values for the critical exponents of different universality classes accompanied by an example of a phase transition are listed in table 3. It should be noted that sufficiently far away from the transition, fluctuations can largely be ignored and mean field behavior prepails. More precisely, corrections to mean field theory can only be expected to become important for temperatures satisfying

$$|t| \lesssim t_G, \tag{11}$$

where

$$t_G = C\left(\frac{k_B}{\Delta c_v \xi_0^d}\right)^{2/(4-d)}. \tag{12}$$

is the Ginzburg scale. Here, d is the effective dimensionality of the system, Δc_v is the jump of the specific heat across the phase transition and ξ_0 is the bare coherence length. In three dimensions, the universal dimensionless proportionality constant C introduced here is given by $C = 1/(32\pi^2)$ [125, 126], which is much smaller than 1.

Quite generally, a crossover is expected near t_G from mean field to non-mean field behavior. If, however, the bare coherence length is sufficiently large, the non-mean field regime can turn out to be unmeasurably small. In conventional superconductors, for example, the size of the bare coherence length can be one thousand the size of the lattice spacing, leading to $t_G \approx 10^{-18}$. As a consequence, mean field theory is essentially exact.

From the experimental point of view, the estimate of critical exponents can be a hard task. For instance, owing to the specific heat critical exponent $\tilde{\alpha}$, a reliable estimate of the phonon background can be one of the crucial points. In addition, for a reliable estimate of the critical behavior of a system, fine measurements close to T_c are necessary. Accurate measurements of e.g. the specific heat are required over several orders of magnitude of t. For real materials, a broadening of the transition due to inhomogeneities (impurities or crystal defects) is frequently observed. Due to this, T_c cannot be measured directly, but is rather obtained indirectly via self consistent fittings.

4.2. Scaling Ansatz for the Mott metal-insulator transition

In 2005, in a stimulating article entitled 'Unconventional Critical Behaviour in a Quasi-2D Organic Conductor', Kagawa and collaborators reported on the criticality at the pressure-induced Mott transition in the organic κ-(BEDT-TTF)$_2$Cu[N(CN)$_2$]Cl charge-transfer salt [45]. In this study, the authors made use of the isothermal pressure-sweep technique, using helium as a pressure transmitting medium, to explore the critical behavior of this organic salt through conductance measurements. The pressure-sweep technique had been previously applied by Limelette and collaborators [127] to study the Mott critical behavior of Cr-doped V_2O_3, which is now recognized as a canonical Mott insulator system and behaves mean-field like. Very close to the transition the authors also claim Ising universality. In contrast to κ-(BEDT-TTF)$_2$Cu[N(CN)$_2$]Cl, chromium-doped vanadium sesquioxide is a truly three-dimensional material. In the study of the quasi-two-dimensional charge-transfer salt κ-(BEDT-TTF)$_2$Cu[N(CN)$_2$]Cl, the critical behavior of the conductance data at the critical endpoint was analyzed in the framework of the scaling theory of the liquid-gas transition [134]. For simplicity, in the so-called non-mixing approximation, the rescaled pressure and the rescaled temperature were used as two independent scaling variables to obtain the critical exponents $\beta = 1$, $\gamma = 1$ and $\delta = 2$, as listed in table 3. Substituting these values in the Rushbrooke relation one obtains $\tilde{\alpha} = -1$. As pointed out by the authors, the obtained critical exponents do not fit in the well-known universality classes, indicating the experimental discovery of a new universality class. A possible explanation of the experimentally observed exponents of unconventional criticality was given by Imada and collaborators [135, 136].

The appearance of unconventional critical exponents came as a surprise to many who expected Ising universality. This expectation was based on an argument by Castellani *et al* [137] who argued that, even though there is no symmetry breaking, the double occupancy of lattice sites can serve as an order parameter. While doubly occupied (or empty) sites are

Table 3. Different universality classes with their respective critical exponents, accompanied by a proposed example of the phase transition. The theoretical estimates for the critical exponents are from [130] (3D Ising), [131] (3D XY) and [132] (3D Heisenberg).

Universality class	$\tilde{\alpha}$	β	γ	δ	Examples of phase transition
Mean-field	0	0.5	1.0	3.0	Superconducting transition in conventional superconductors or Mott MI transition in $(V_{1-x}Cr_x)_2O_3$ [127]
2D Ising	0	0.125	1.75	15	Preroughening transition in GaAs [128]
3D Ising	0.110(1)	0.3265(3)	1.2372(5)	4.789(2)	Liquid-gas transition
3D XY	−0.0151(3)	0.3486(1)	1.3178(2)	4.780(1)	Superfluid transition in ^{4}He [129]
3D Heisenberg	−0.1336(15)	0.3689(3)	1.3960(9)	4.783(3)	Ferromagnetic transition in a clean and isotropic ferromagnet
Unconventional criticality	−1	1	1	2	Mott MI transition in κ-(BEDT-TTF)$_2$Cu[N(CN)$_2$]Cl [45]

Note: The mean-field values are derived in any textbook on critical phenomena (see e.g. [121–124]), values quoted for the 2D Ising model are the exact values from Onsager's famous solution [133].

localized on the insulating side of the phase transition, they do proliferate on the metallic site. The order parameter was therefore expected to be of an Ising type. The Mott criticality was also studied in the framework of dynamical mean-field theory of the Hubbard model by Kotliar *et al* [140]. These authors confirmed the statement that the Mott transition should lie in the Ising universality class. Having a phase transition between a low-density gas of localized doubly occupied or empty lattice sites to a high-density fluid of unbound doubly occupied or empty lattice sites is quite analogous to the well-known liquid-gas transition which lies also in the Ising universality class.

An attempt to reconcile the experimentally observed unconventional critical exponents $\beta = 1$, $\gamma = 1$ and $\delta = 2$ with the well-established two-dimensional Ising universality class was made by Papanikolaou and collaborators [46]. These authors pointed out that the critical exponents derived from transport measurements do not necessarily coincide with the thermodynamic critical exponents which are defined in terms of an order parameter. According to Papanikolaou *et al* [46], the singular part of the conductivity $\Delta\Sigma$ does not only depend on the singular part of the order parameter, but also depends on the related energy density. As a consequence, $\Delta\Sigma$ is given by

$$\Delta\Sigma = Am + \mathrm{sgn}(m)B|m|^{\theta}. \tag{13}$$

Here, A and B are non-universal coefficients, m is the order parameter and $\theta = (1-\tilde{\alpha})/\beta$. In an extended regime not too close to the critical point the first term on the r.h.s. can be much smaller than the second one such that

$$\Delta\Sigma \propto \mathrm{sgn}(m)|m|^{\theta}. \tag{14}$$

It then follows that the critical exponents as obtained from the conductivity can be expressed in terms of the thermodynamic critical exponents as follows [46]: $\beta_\sigma = \theta\beta$, $\delta_\sigma = \delta/\theta$ and $\gamma_\sigma = \gamma + \beta(1-\theta)$. In particular, for the 2D Ising universality class one obtains with $\theta = 8$ the exponents $\beta_\sigma = 1$, $\delta_\sigma = 7/4$ and $\gamma_\sigma = 7/8$ which within the experimental resolution are consistent with the exponents obtained by Kagawa *et al* [45].

To explain the lattice response in the vicinity of the MI finite temperature critical end point and explain the corresponding peak in the thermal expansivity a description in terms of critical exponents is not sufficient unless the pressure is tuned to its critical value. Instead, the usage of a scaling theory was proposed in [4]. While such an approach is extremely general and can be applied to any universality class, it was shown in [4] that the expansivity data of [2] is in fact consistent with 2D Ising criticality: Within the scenario of two-parameter scaling, the Gibbs free energy can be written as

$$f(t,h) = |h|^{d/y_h}\Phi\left(t/|h|^{y_t/y_h}\right). \tag{15}$$

Here, $\Phi(x)$ is a universal scaling function which only depends on the universality class, t and h are the two (suitably normalized) scaling variables and y_t and y_h are their corresponding RG eigenvalues. These are the two relevant eigenvalues of the underlying universality class and determine all critical exponents. For example, $\tilde{\alpha} = 2 - d/y_t$ or $\beta = (d - y_h)/y_t$ (see e.g. [121–124]). Conventionally, $t = (T - T_c)/T_0$ and $h = (P - P_c)/P_0$ can be thought of as temperature- and pressure-like quantities, but more generally there are also linear mixing terms such that $t = (T - T_c - \zeta(P - P_c))/T_0$ and $h = (P - P_c - \lambda(T - T_c))/P_0$. In fact, very close to the transition Hooke's law of elasticity breaks down and one should expect compressive strain to enter linearly the scaling variables instead of pressure, see below and [5].

The appearance of the mixing terms is a consequence of the experimental fact that the first-order transition line ending in the critical point (P_c, T_c) is not parallel to the T axis, see figure 7. While the linear mixing terms turn out to be important for a quantitative description of the expansivity data [4], let us for simplicity focus here on the much simpler case of no mixing. For the 2D Ising universality class, $y_t = 1$ and $y_h = 15/8$. Having one integer-valued RG eigenvalue, logarithmic corrections to scaling should be expected [122]. As it turns out, the scaling ansatz for the 2D Ising universality class requires a correction term and reads [138]

$$f(t,h) = \frac{t^2}{8\pi}\ln t^2 + |h|^{d/y_h}\Phi\left(t/|h|^{y_t/y_h}\right). \tag{16}$$

Differentiating twice with respect to t and setting h equal to zero one then obtains the well-known logarithmic divergence of the specific heat α_{sing}. Assuming no mixing terms, the singular part of the thermal expansivity is given by [46]

$$\alpha_{\mathrm{sing}}\Big|_{h=\pm 0} \propto \frac{\partial^2 f}{\partial h\,\partial t}\Big|_{h=\pm 0} \propto \mathrm{sgn}(h)\,(-t)^{-1+\beta}, \quad t < 0. \tag{17}$$

As a consequence, the Grüneisen ratio $\Gamma_{\rm sing} = \alpha_{\rm sing}/c_{\rm sing}$ diverges for $t < 0$ as [4]

$$\Gamma_{\rm sing} = \left.\frac{\alpha_{\rm sing}}{c_{\rm sing}}\right|_{h=\pm 0} \propto \mathrm{sgn}\,(h)\,(-t)^{-1+\tilde{\alpha}+\beta}. \qquad (18)$$

Let to emphasize here that the true divergence of the Grüneisen parameter is a consequence of neglecting linear mixing terms. Including such mixing terms effectively leads to a saturation of the Grüneisen parameter at a very large value. It was estimated in [4] that the crossover scale for the D8-Br crystals is of order 0.1 bar and thus for most practical purposes beyond experimental resolution. The smallness of this crossover scale can be related via the Clausius–Clapeyron equation to comparatively small entropy differences between the metallic and insulating phases.

The Grüneisen ratio is also known to diverge at a quantum critical point [139].

In the case $\tilde{\alpha} < 0$ there is no divergence in the specific heat, implying that the specific heat is bounded and can safely be replaced by a constant. This has interesting consequences for the universality class of unconventional criticality for which $\tilde{\alpha} = -1$ and $\beta = 1$. In this case both the expansivity and the specific heat stay finite such that there is no divergence of the Grüneisen ratio. Still, there is no reason to expect the expansivity to be proportional to the specific heat, i.e. Grüneisen scaling breaks down [4].

To describe the expansivity of the κ-ET salts away but close to criticality, i.e. for $h \neq 0$, we can express the singular part of the expansivity in terms of derivatives of the scaling function $\Phi(x)$. Differentiating equation (16) with respect to t and h, one obtains [4]

$$\alpha_{\rm sing}(t, h) \propto \mathrm{sgn}(h)\,|h|^{-1+(d-y_t)/y_h}\,\Psi_\alpha(t/|h|^{y_t/y_h}), \qquad (19)$$

with the scaling function $\Psi_\alpha(x)$ given by

$$\Psi_\alpha(x) = \frac{d-y_t}{y_h}\Phi'(x) - \frac{y_t}{y_h}x\Phi''(x). \qquad (20)$$

Even though the 2D Ising model can be solved exactly, there is no known exact expression for the scaling function $\Phi(x)$ and hence no exact expression for $\Psi_\alpha(x)$. Nevertheless $\Phi(x)$ [and hence $\Psi_\alpha(x)$] can be calculated with very high accuracy numerically [4, 138], for a plot see figure 25. With this scaling function at hand, the singular part of the thermal expansivity can now be plotted as a function of t and h, see figure 26. This singular part of the thermal expansivity corresponds to the critical region in the pressure-temperature phase diagram. The first-order transition line is simply represented by the jump in $\alpha_{\rm sing}(t, h)$ for $h = 0$ and $t < 0$ which describes the change in volume $\Delta V \propto (-t)^\beta$. It should be noted that every cut of the graph for constant h is just a rescaled version of the scaling function $\Psi_\alpha(x)$, as shown graphically in figure 25. Also, the change of sign of $\alpha_{\rm sing}$ with a change of sign of h can clearly be seen. While a constant pressure corresponds to a constant h in the non-mixing approximation, in the case of linear mixing terms a constant P corresponds to cutting the graph in figure 26 at an angle. Fitting the thermal expansivity of the D8-Br crystals [2] # 1 and # 3 by a scaling

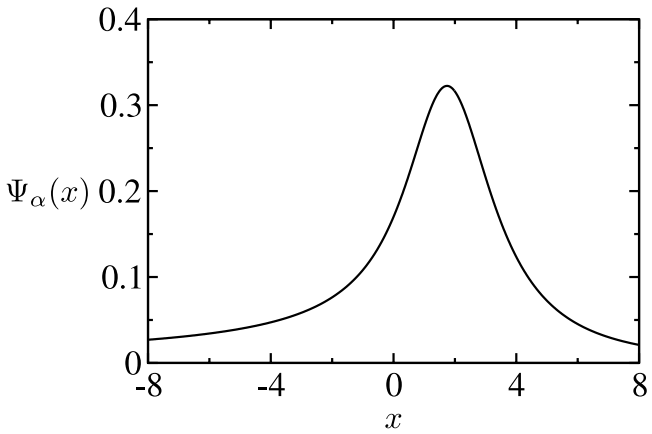

Figure 25. Plot of the scaling function $\Psi_\alpha(x)$ of the thermal expansivity for the 2D Ising universality class. Figure reproduced from [4].

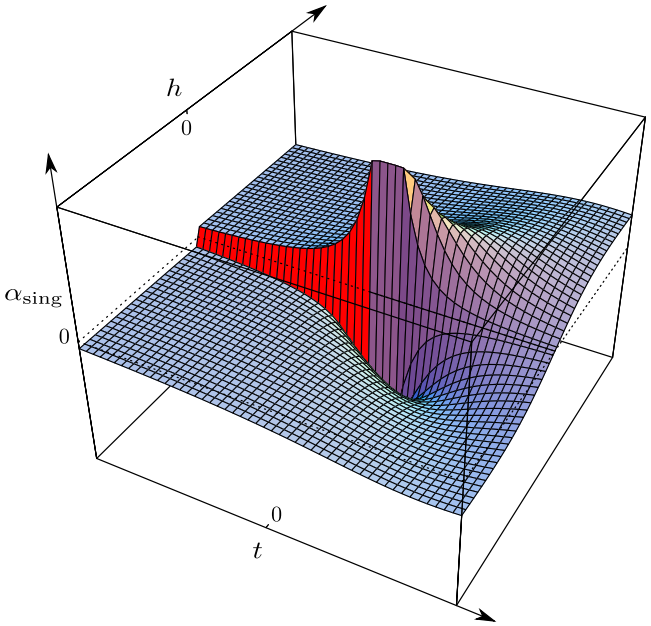

Figure 26. Plot of the singular part of the thermal expansivity $\alpha_{\rm sing}$ as a function of the scaling variables t and h. The first-order transition line along the negative t-axis manifests itself by a jump in the expansivity which for $t \to 0$ diverges as $\Delta\alpha_{\rm sing} \propto (-t)^{-1+\beta} = (-t)^{-7/8}$, see equation (17). It should be noted that every cut at constant h is just given by the (rescaled) scaling function $\Psi_\alpha(x)$, as graphically depicted in figure 25. Figure reproduced from [4].

form of the thermal expansivity based on equation (19) on top of a linear background including linear mixing terms gives indeed an excellent fit for the Ising universality class [4], see figure 27.

Even though the Ising universality class leads to an excellent fit of the dilatometric data, we would like to stress here that this is by far no proof of Ising universality. NMR mearsurements of $1/TT_1$ obey roughly $\Delta(1/TT_1) \propto (P - P_c)^{1/\delta}$, with $\delta \approx 2$, as also obtained from conductance measurements [45]. As far as we know, the NMR measurements have not found a natural explanation based on Ising criticality yet.

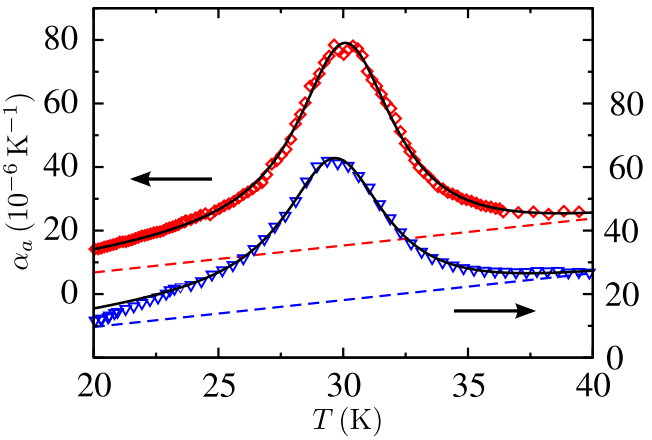

Figure 27. Fit of the expansivity data of the two D8-Br crystals # 1 (diamonds ◊) and # 3 (triangles ∇) from [2] to the scaling theory outlined in the text. In total, there are six fitting parameters involved. Two fitting parameters determine the height and width of the peak, two fitting parameters determine the orientation of the temperature and pressure axes (and thereby describes linear mixing terms) and finally two fitting parameters are necessary to describe the analytic background contribution, as described by the dashed line. Figure reproduced from [4].

Notwithstanding the analogy between the Mott MI and the liquid-gas transition, differences do exist and the compressible MI with its long-range shear forces should rather be classified as a solid–solid transition [5]. Hopping matrix integrals do depend on the distance between neighboring atoms, such that the Mott MI transition is sensitive to elastic strain and couples only indirectly to the applied stress, e.g. compressive pressure. As described in detail in [5] and similarly also in the context of the compressible Hubbard model in [51], the homogeneous component E of the strain can be obtained by minimizing the effective potential density

$$V(E) = \frac{K_0}{2}E^2 - (P - P_0)E + f_{\mathrm{sing}}(t(T, E), h(T, E)), \tag{21}$$

where both $t(T, E)$ and $h(T, E)$ are linear functions of T and E, K_0 is the bare bulk modulus and P_0 is an offset pressure. For simplicity, we have replaced all tensorial quantities by scalars. It was shown in [5] that while not too close to the critical end point Hooke's law holds and our above treatment was legitimate, the feedback of the electronic subsystem back on the lattice drives the effective bulk modulus to zero even above the phase transition described by f_{sing} alone, thereby leading to a violation of Hooke's law and a preempted phase transition. This phase transition was explicitly shown to be governed by Landau criticality with mean-field exponents.

While there is no final answer on the universality class underlying the Mott transition in the κ-ET charge-transfer salts yet, we hope that future experiments will shed more light on this issue.

5. Thermal expansion measurements on κ-(ET)$_2$Cu$_2$(CN)$_3$

The thermal expansion coefficient along the in-plane c-axis for crystal #1 of the salt κ-(ET)$_2$Cu$_2$(CN)$_3$ is shown in figure 28.

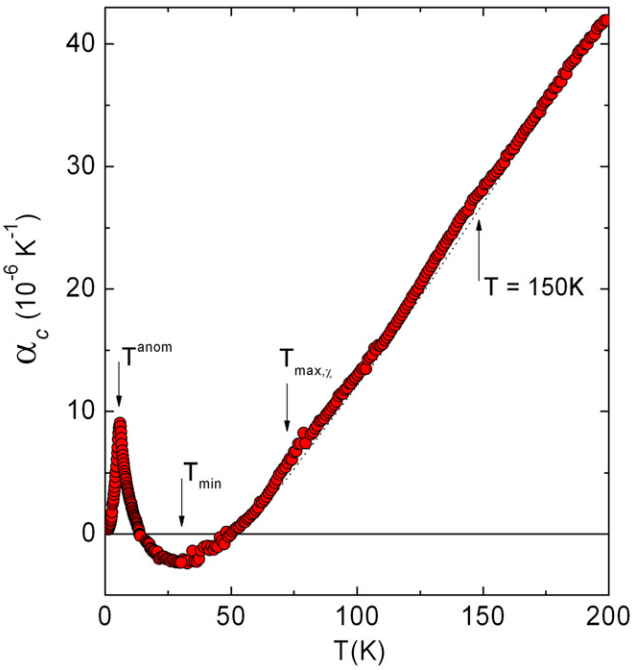

Figure 28. Expansivity along the in-plane c-axis for a single crystal of κ-(ET)$_2$Cu$_2$(CN)$_3$. T^{anom} indicates the temperature at which, according to [6], the crossover (hidden ordering) to a spin-liquid state occurs. The dashed line is used to indicate a hypothetical linear background. Broad hump anomalies at $T \simeq 150$ K and $T_{\mathrm{max},\chi} \simeq 70$ K are indicated by the arrows, see the discussion in the text. Figure taken from [3].

Recall that this is the spin-liquid candidate. Upon cooling, α_c decreases monotonously down to $T_{\mathrm{min}} \simeq 30$ K. Around $T = 150$ K, indications of a small and broad hump are observed. In [8], Shimizu and collaborators observed an enhancement of the spin relaxation rate above 150 K, which was attributed to the freezing of the thermally activated vibration of the ethylene end groups. Note that no traces of a glass-like anomaly around $T = 77$–80 K are observed. This behavior is quite distinct from that observed in κ-(ET)$_2$Cu[N(CN)$_2$]Cl (see [25]) and κ-D8-Br (discussed in section 3) and κ-H8-Br [25], where clear signatures in the thermal expansion coefficient show up at $T_g \simeq 77$ K. This discrepancy indicates that the lattice dynamic for the κ-(ET)$_2$Cu$_2$(CN)$_3$ salt is different from that of the above-mentioned compounds. In fact, according to the RUM model, introduced in section 3.1, the absence of a glass-like anomaly in the κ-(ET)$_2$Cu$_2$(CN)$_3$ salt can be understood in the following way: the anion Cu$_2$(CN)$_3^-$ (figure 6) consists of a 2D network of Cu(I) and bridging cyanide groups [33]. As the Cu$_2$(CN)$_3^-$ anion is arranged in a network fashion, which is quite different from the polymeric arrangement of Cu[N(CN)$_2$]Cl$^-$ and Cu[N(CN)$_2$]Br$^-$ (figure 5), the vibration modes of the CN groups are confined between nearest Cu(I) atoms, so that they cannot propagate along the structure. Hence, the formation of RUM in κ-(ET)$_2$Cu$_2$(CN)$_3$ is very unlikely and as a consequence no signatures of the glass-like transition can be observed. Cooling the system further, another broad hump is observed at $T_{\mathrm{max},\chi} \simeq 70$ K. The latter coincides roughly with a broad maximum observed in magnetic susceptibility measurements [8]. Below $T \simeq 50$ K,

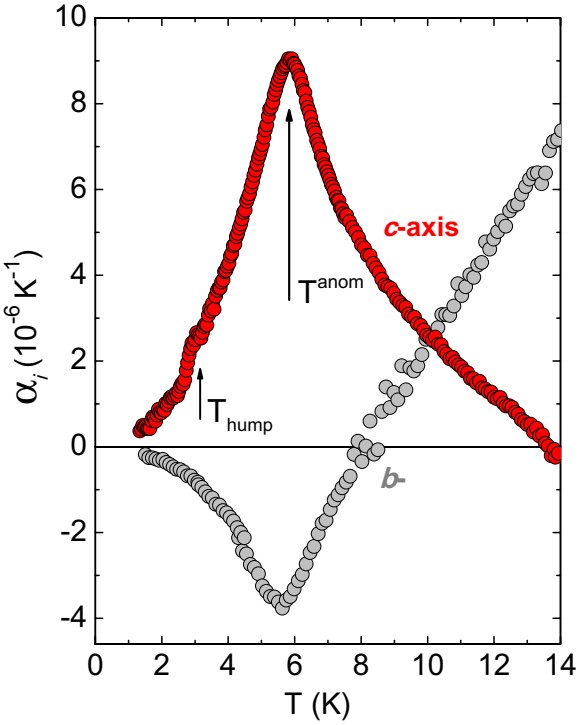

Figure 29. Blow-up of the low-temperature expansivity data along the in-plane c- (crystal #1) and b-axis (crystal #2) of κ-$(ET)_2Cu_2(CN)_3$ on expanded scales, showing the sharpness of the transition at $T^{anom} \simeq 6$ K and a hump in α_c at $T_{hump} \simeq 2.8$ K along the c-axis. Figure taken from [3], see also [76].

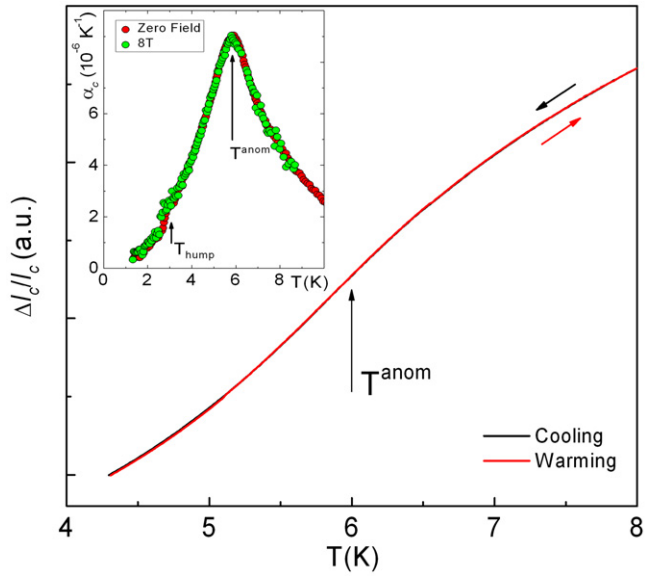

Figure 30. Main panel: relative length changes (in arbitrary units) for κ-$(ET)_2Cu_2(CN)_3$ along the in-plane c-axis measured at very low sweep-rate of ± 1.5 K h^{-1}, showing the absence of hysteretic behavior. Inset: thermal expansion data under zero magnetic field and 8 T. Such measurements were taken on warming, with the magnetic field applied at 1.3 K. Figure taken from [3].

α_c assumes negative values. Cooling the system further, a broad minimum is observed at $T_{min} \simeq 30$ K. Below $T \simeq 14$ K, α_c starts to assume positive values. A possible scenario for explaining the negative thermal expansion in the temperature range $14\,\text{K} \lesssim T \lesssim 50\,\text{K}$ is discussed in the following. In this temperature range, lattice vibration modes (most likely from the anion) become soft, the Grüneisen parameter in turn assumes negative values and the lattice expands upon cooling. Interestingly enough, negative thermal expansion has been also observed in amorphous $Y_{100-x}Fe_x$ (x = 92.5 and 84) alloys over the temperature range in which these systems go from the paramagnetic to the spin-glass state. The latter feature is assigned to the thermal dependence of the spin fluctuations [141]. Thus, for the spin-liquid candidate the hypothesis of negative thermal expansion driven by spin degrees of freedom cannot be ruled out. In fact, the connection between negative thermal expansion and frustration has been reported in the literature, but a theory able to describe these phenomena is still lacking [142]. Upon further cooling, a huge anomaly is observed at $T^{anom} \simeq 6$ K. The latter coincides with the hump anomaly observed in specific heat measurements [6]. This finding constitutes the first observation of lattice effects associated with the transition (or crossover/hidden ordering) at 6 K. A further analysis of the present data is difficult because the actual phonon background cannot be estimated. The low-temperature data will be discussed in more detail in the following. figure 29 shows the thermal expansion coefficient below 14 K on expanded scales.

Upon cooling below 6 K, a hump at $T \simeq 2.8$ K is observed. Several runs were performed in order to check for reproducibility. The latter feature has not been observed in specific heat measurements [6], most likely due to the lack of resolution of such experiments.

The signatures observed in α_c have their direct correspondence in the spin-lattice relaxation rate (T_1^{-1}) and magnetic susceptibility (χ) [8]. Below 50 K, both quantities decrease monotonously with temperature down to 4 K, where T_1^{-1} starts to increase and shows a broad maximum at 1 K, while χ varies smoothly [8]. Thermal expansion measurements under magnetic fields (inset of figure 30) revealed that under 8 T, the peak position around 6 K as well as the hump at $T \simeq 2.8$ K remain unaltered, in agreement with specific heat measurements under a magnetic field [6], indicating that the anomaly at 6 K is unlikely to be due to long-range magnetic ordering, at least for magnetic fields applied parallel to the c-axis. At this point, it is worthwhile mentioning that for the 'spin ice' system $Dy_2Ti_2O_7$ [111], already mentioned previously, the spins' disorder is suppressed when a magnetic field is applied perpendicular to their Ising axis. In addition, measurements on cooling and warming (main panel of figure 30) revealed no traces of hysteretic behavior, at least in the resolution of the present experiments, so that the hypothesis of a first-order transition can be ruled out.

Hence, the actual origin of the anomaly in α_c at 6 K remains unclear. However, at first glance, the present thermal expansion findings appear to fit in the model proposed by Lee *et al* [65], which we described briefly at the end of the introduction. According to this model, spin pairing on the Fermi surface generates a spontaneous breaking of the lattice symmetry, giving rise to a phase transition at finite temperature, which in turn is coupled to a lattice distortion. In other words, upon cooling, the spin entropy has to be (partially) frozen. The only way for this, without long-range

magnetic ordering, is to introduce a lattice distortion. This process presents some similarities with a classical Spin-Peierls transition, where the formation of a singlet state requires that the spin entropy of the triplet state goes to zero by introducing a lattice distortion. In the present case, the amount of entropy in the temperature range $0.3\,\mathrm{K} < T < 1.5\,\mathrm{K}$ corresponds to only a few percent of $R \ln 2$ [6], indicating therefore that only a minor part of the total number of spins contribute to the spin-liquid phase. Interestingly enough, the shape of the transition at 6 K (figure 29) resembles the shape of the anomaly in the thermal expansion coefficient associated with the Spin-Peierls transition for the quasi-1D organic conductors $(TMTTF)_2X$ ($X = PF_6$ and AsF_6) [74]. Hence, the sharp lattice distortion at $T^{\mathrm{anom}} \simeq 6\,\mathrm{K}$ seems to be associated with a real phase transition and not with a crossover, as proposed in [6]. In fact, thermal expansion measurements along the second in-plane b-axis revealed striking anisotropic in-plane lattice effects [76]. Interestingly enough, along the in-plane b-axis (see figure 29) a negative anomaly is observed at $T^{\mathrm{anom}} \simeq 6\,\mathrm{K}$, indicating that below T^{anom} a lattice expansion (shrinkage) along the c-axis (b-axis) occurs. The observed distinct in-plane anisotropy implies that the hopping integral terms t and t' are strongly affected.

It remains to be seen whether κ-$(ET)_2Cu_2(CN)_3$ is in fact in a spin-liquid state for $T \to 0$. In this sense, thermal expansion measurements at very low temperatures along the a-, b- and c-axes are required in order to achieve a better understanding of the physics of this exciting material. Such experiments will reveal, for example, whether below 1.3 K α/T behaves linearly and remains finite as $T \to 0$, as observed in specific heat measurements [6] or if α/T decreases exponentially. As already mentioned at the end of the introduction, it was more recently reported [66] that the thermal conductivity of κ-$(ET)_2Cu_2(CN)_3$ is described by an activated behavior with a gap $\Delta_\kappa \simeq 0.46\,\mathrm{K}$. The latter results are at odds with the specific heat measurements performed by Yamashita *et al* [6]. Based on such results, one can see that a full picture of the fundamental aspects of the spin-liquid phase in κ-$(ET)_2Cu_2(CN)_3$ is still incomplete and requires further investigations.

6. Conclusions and perspectives

In this review, we have addressed one of the central questions in the field of strongly correlated electron systems, whether lattice degrees of freedom play a role for several physical phenomena, among them the Mott MI transition. Molecular conductors of the κ-$(BEDT\text{-}TTF)_2X$ family have been revealed as model systems for the study of the latter phenomena. The main findings discussed in this review are summarized below.

High-resolution thermal expansion measurements on fully deuterated salts of κ-$(BEDT\text{-}TTF)_2Cu[N(CN)_2]Br$ revealed pronounced lattice effects at the Mott metal-to-insulator transition temperature $T_{\mathrm{MI}} = 13.6\,\mathrm{K}$, accompanied by a striking anisotropy. While huge effects are observed along the in-plane a-axis, along which the polymeric anion chains are aligned, an almost zero effect is observed along the second in-plane c-axis, along which the polymeric anion chains are linked via Br-N weak contacts. Still more amazing is the observation of pronounced lattice effects along the out-of-plane b-axis. These findings provide strong evidence that the Mott transition for the present class of materials cannot be fully understood in the frame of a purely 2D electronic triangular dimer model. Even though there is still an ongoing debate about the universality class and possible crossover scales of the Mott transition, the scaling theory reviewed here can be used with any universality class. Candidates suggested for the Mott transition in the κ-ET salts are unconventional criticality [45, 135, 136], 2D Ising [46] and a crossover to Landau criticality [5]. It was explicitly shown that the thermal expansivity data for the κ-D8-Br salt is consistent with 2D Ising criticality [4], which of course does not provide a proof of this universality class. Finally, the experimentally observed critical exponent $\delta = 2$ was also argued to be due to subleading quantum effects preceding an asymptotic critical regime [143].

In order to achieve a better understanding of the Mott transition in the present material, thermal expansion measurements were taken under magnetic field, quasi-uniaxial pressure as well as by employing different cooling speeds across the glass-like transition. For example, measurements under magnetic field reveal that the Mott MI insulator transition temperature is insensitive to magnetic fields up to 10 T, which is in agreement with the picture of a Mott insulator with a hole localized on a dimer formed by an ET molecule. A magnetic field-induced first-order phase transition at $T_{\mathrm{SF}} \simeq 9.5\,\mathrm{K}$ for a field applied along the out-of-plane b-axis was observed, indicative of a spin-flop transition with strong magneto-elastic coupling. Measurements under quasi-uniaxial pressure applied along the out-of-plane b-axes revealed effects in contrast to those observed upon increasing the cooling speed across the glass-like transition. While quasi-uniaxial pressure shifts T_{MI} towards lower temperatures and T_p to higher temperatures, the opposite situation is observed upon fast cooling through the glass-like transition. Interestingly enough, the so-called glass-like transition temperature T_g remains unaffected under quasi-uniaxial pressure. Although by means of thermal expansion measurements one has access to the macroscopic behavior of the sample studied, the strong anisotropic lattice effects observed, marked by a negative thermal expansion above T_g, enable us to draw some conclusions at the microscopic level. Hence, a model within the rigid-unit-mode scenario, taking into account the low-energy vibration modes of the cyanide ligands of the polymeric anions $Cu[N(CN)_2]Br^-$, was proposed to describe the negative thermal expansion above the $T_g \simeq 77\,\mathrm{K}$. In this model, low-energy vibration modes of the cyanide groups of the polymeric anion chains become frozen upon cooling down to T_g, shrinking thus the a lattice parameter upon warming the system above T_g.

Additional experiments, including magnetostriction measurements both above and below the magnetic field-induced phase transition temperature T_{FI} as well as magnetic measurements with B thoroughly aligned along the out-of-plane b-axis, will certainly help to achieve a better

understanding of the behavior of almost localized correlated electrons in this interesting region of the phase diagram of the κ-phase of (BEDT-TTF)$_2$X charge-transfer salts. A theoretical study of the stability of the Mott insulating state and the neighboring superconducting phase, taking into account magnetic field-induced lattice effects, is highly desired as well. We have here presented a phenomenological description of the Mott metal-insulator transition within a scaling theory. While transport measurements revealed unconventional critical exponents, it would be desirable to have direct access to thermodynamic quantities. In particular, we hope that future expansivity measurements under pressure might give rise to a better understanding.

We have also examined in this review thermal expansion measurements on the κ-(BEDT-TTF)$_2$Cu$_2$(CN)$_3$ salt, a system which is proposed as a candidate for the realization of a spin-liquid ground state. Measurements taken along the in-plane c-axis reveal some interesting aspects, which can be of extreme importance for a wider understanding of the physical properties of this material. For example, the absence of the so-called glass-like transition in κ-(BEDT-TTF)$_2$Cu$_2$(CN)$_3$ is in line with the above-mentioned model within the rigid-unit modes scenario. While the anion Cu[N(CN)$_2$]Br$^-$ is arranged in form of chains weakly linked via Br-N contacts, the anions $Cu_2(CN)_3^-$ are arranged in a 2D network fashion, so that the cyanide groups are confined between the Cu atoms and therefore the vibration modes associated with the cyanide groups cannot propagate along the structure as it occurs, for example, in fully deuterated salts of κ-(BEDT-TTF)$_2$Cu[N(CN)$_2$]Br, see the discussion above. A negative thermal expansion is observed in the temperature range $14 < T < 50$ K. In addition, the thermal expansion coefficient reveals a huge anomaly, indicative of a phase transition at $T = 6$ K, coinciding nicely with a hump in the specific heat, which has been assigned to a crossover to the quantum spin-liquid state. Last but not least, during the preparation of the final version of this article, a theoretical treatment for the thermal expansivity of the charge-transfer salts of the κ-(BEDT-TTF)$_2$X family based on electronic correlations was proposed by Kokalj and McKenzie [144]. These authors consider both the dependence of the system entropy on the Hubbard parameters U, t, t' and the dependence with temperature of the double occupancy and bond-orders to describe the thermal expansion of these materials.

Acknowledgments

We would like to thank A Brühl, M Dressel, R M Fernandes, M Garst, A A Haghighirad, K Kanoda, S Köhler, P Kopietz, R S Manna, R E L Monaco, J Müller, R Paupitz, J-P Pouget, B Powell, T Sasaki, J A Schlueter, J Schmalian, D Schweitzer, A C Seridonio, C Strack, R Urbano, B Wolf, M Zacharias and in particular M Lang for valuable discussions and collaborations along the years. MdS acknowledges financial support from the DFG via SFB/TRR 49, São Paulo Research Foundation—Fapesp (Grant No. 2011/22050-4) and National Counsel of Technological and Scientific Development—CNPq (Grant No. 308977/2011-4).

References

[1] Kawamoto A, Miyagawa K and Kanoda K 1997 *Phys. Rev.* B **55** 14140
[2] de Souza M, Brühl A, Strack C, Wolf B, Schweitzer D and Lang M 2007 *Phys. Rev. Lett.* **99** 037003
[3] de Souza M 2008 *PhD Thesis* University of Frankfurt, Germany (http://publikationen.ub.uni-frankfurt.de/volltexte/2009/6240/)
[4] Bartosch L, de Souza M and Lang M 2010 *Phys. Rev. Lett.* **104** 245701
[5] Zacharias M, Bartosch L and Garst M 2012 *Phys. Rev. Lett.* **109** 176401
[6] Yamashita S, Nakazawa Y, Oguni M, Oshima Y, Nojiri H, Shimizu Y, Miyagawa K and Kanoda K 2008 *Nat. Phys.* **4** 459
[7] Jeschke H O, de Souza M, Valentí R, Manna R S, Lang M and Schlueter J A 2012 *Phys. Rev.* B **85** 035125
[8] Shimizu Y, Miyagawa K, Kanoda K, Maesato M and Saito G 2003 *Phys. Rev. Lett.* **91** 107001
[9] Balents L 2010 *Nature* **464** 199
[10] Lang M 1996 *Supercond. Rev.* **2** 1
[11] Lang M and Müller J 2004 Organic superconductors *The Physics of Superconductors* vol 2, ed K H Bennemann and J B Ketterson (Berlin: Springer) p 435–554
[12] Ishiguro T and Yamaji K 1990 *Organic Superconductors* (*Springer Series in Solid-State Sciences* vol 88) (Germany: Springer)
[13] Jérome D 1991 The physics of organic superconductors *Science* **252** 1509
[14] McKenzie R H 1998 *Comment. Condens. Matter Phys.* **18** 309–37
[15] Wosnitza J 2000 *Studies of High Temperature Superconductors* vol 34 (New York: Nova Science Publishers) pp 97–131
[16] Singleton J 2002 *J. Solid State Chem.* **168** 675
[17] Miyagawa K, Kanoda K and Kawamoto A 2004 *Chem. Rev.* **104** 5635–53
[18] Fukuyama H 2006 *J. Phys. Soc. Japan* **75** 051001
[19] Mori H 2006 *J. Phys. Soc. Japan* **75** 051003
[20] Kanoda K 2006 *J. Phys. Soc. Japan* **75** 051007
[21] Powell B J and McKenzie R H 2006 *J. Phys.: Condens. Matter* **18** R827–66
[22] Toyota N, Lang M and Müller J 2007 *Low-Dimensional Molecular Metals* (Germany: Springer)
[23] Kanoda K and Kato R 2011 *Annu. Rev. Condens. Matter Phys.* **2** 167
[24] Powell B J and McKenzie R H 2011 *Rep. Prog. Phys.* **74** 056501
[25] Müller J, Lang M, Steglich F, Schlueter J A, Kini A M and Sasaki T 2002 *Phys. Rev.* B **65** 144521
[26] Sasaki T, Yoneyama N, Kobayashi N, Ikemoto Y and Kimura H 2004 *Phys. Rev. Lett.* **92** 227001
[27] Salameh B 2005 *PhD Thesis* University of Stuttgart, Germany
[28] Kandpal H C, Opahle I, Zhang Y-Z, Jeschke H O and Valenti R 2009 *Phys. Rev. Lett.* **103** 067004
[29] Nakamura K, Yoshimoto Y, Kosugi T, Arita R and Imada M 2009 *J. Phys. Soc. Japan* **78** 083710
[30] Schlueter J A, Geiser U, Whited M A, Drichko N, Salameh B, Petukhov K and Dressel M 2007 *Dalton Trans.* **2007** 2580
[31] Schlueter J A, Wiehl L, Park H, de Souza M, Lang M, Koo H J and Whangbo M H 2010 *J. Am. Chem. Soc.* **132** 16308
[32] Kini A M 1990 *Inorg. Chem.* **29** 2555
[33] Geiser U *et al* 1991 *Inorg. Chem.* **30** 2586
[34] Geiser U *et al* 1991 *Physica* C **174** 475
[35] Kanoda K 1997 *Hyperfine Interact.* **104** 235
[36] Mckenzie R H 1997 *Science* **278** 820
[37] Dagoto E 2005 *Science* **309** 257

[38] Taylor O J, Carrington A and Schlueter J A 2007 *Phys. Rev. Lett.* **99** 057001
[39] Lefebvre S, Wzietek P, Brown S, Bourbonnais C, Jérome, Méziere C, Fourmigué M and Batail P 2000 *Phys. Rev. Lett.* **85** 5420
[40] Nam M-S, Ardavan A, Blundell S J and Schlueter J A 2007 *Nature* **449** 584
[41] Limelette P, Wzietek P, Florens S, Georges A, Costi T A, Pasquier C, Jérome D, Mézière C and Batail P 2003 *Phys. Rev. Lett.* **91** 016401
[42] Fournier D, Poirier M, Castonguay M and Truong K D 2003 *Phys. Rev. Lett.* **90** 127002
[43] Lang M, de Souza M, Brühl A, Strack C, Wolf B, Schlueter J A, Müller J and Schweitzer D 2007 *Proc. of the 8th Int. Conf. on Materials and Mechanisms of Superconductivity: High Temperature Superconductors (Dresden, Germany, 1 September 2007)* (Physica C) vol 460–2 p 129
[44] Kagawa F, Itou T, Miyagawa K and Kanoda K 2004 *Phys. Rev.* B **69** 064511
[45] Kagawa F, Miyagawa K and Kanoda K 2005 *Nature* **436** 534
[46] Papanikolaou S, Fernandes R M, Fradkin E, Phillips P W, Schmalian J and Sknepnek R 2008 *Phys. Rev. Lett.* **1** 026408
[47] Lunkenheimer P *et al* 2012 *Nat. Mater.* **11** 755
[48] Kurosaki Y, Shimizu Y, Miyagawa K, Kanoda K and Saito G 2005 *Phys. Rev. Lett.* **95** 177001
[49] Strack C *et al* 2005 *Phys. Rev.* B **72** 054511
[50] Kawamoto A, Miyagawa K, Nakazawa Y and Kanoda K 1995 *Phys. Rev.* B **52** 15522
[51] Hassan S R, Georges A and Krishnamurthy H R 2005 *Phys. Rev. Lett.* **94** 036402
[52] Merino J and McKenzie R H 2000 *Phys. Rev.* B **62** 16442
[53] Singleton J, Goddard P A, Ardavan A, Harrison N, Blundell S J, Schlueter J A and Kini A M 2002 *Phys. Rev. Lett.* **88** 037001
[54] Welp U, Fleshler S, Kwok W K, Crabtree G W, Carlson K D, Wang H H, Geiser U, Williams J M and Hitsman V M 2000 *Phys. Rev. Lett.* **69** 840
[55] Pinterić M, Miljak M, Biškup N, Milat O, Aviani I, Tomić S, Schweitzer D, Strunz W and Heinen I 2000 *Eur. Phys. J.* B **11** 217
[56] Miyagawa K, Kawamoto A, Nakazawa Y and Kanoda K 1995 *Phys. Rev. Lett.* **75** 1174
[57] Kagawa F, Itou T, Miyagawa K and Kanoda K 2004 *Phys. Rev. Lett.* **93** 127001
[58] Smith D F, De Soto S M, Slichter C P, Schlueter J A, Kini A M and Daugherty R G 2000 *Phys. Rev.* B **68** 024512
[59] Smith D F, Slichter C P, Schlueter J A, Kini A M and Daugherty R G 2004 *Phys. Rev. Lett.* **93** 167002
[60] Kawamoto A, Yamasita M and Kumagai K-I 2004 *Phys. Rev.* B **70** 212506
[61] Miyagawa K, Kawamoto A and Kanoda K 2002 *Phys. Rev. Lett.* **89** 017003
[62] Anderson P W 1973 *Mater. Res. Bull.* **8** 153
[63] Anderson P W 1987 *Science* **235** 1196
[64] Ramirez A P 2008 *Nat. Phys.* **4** 442
[65] Lee S-S, Lee P A and Senthil T 2007 *Phys. Rev. Lett.* **98** 067006
[66] Yamashita M, Nakata N, Kasahara Y, Sasaki T, Yoneyama N, Kobayashi N, Fujimoto S, Shibauchi T and Matsuda Y 2009 *Nat. Phys.* **5** 44
[67] Qi Y, Xu C and Sachdev S 2009 *Phys. Rev. Lett.* **102** 176401
[68] Pratt F L, Baker P J, Blundell S J, Lancaster T, Ohira-Kawamura S, Baines C, Shimizu Y, Kanoda K, Watanabe I and Saito G 2011 *Nature* **471** 612
[69] Hartke K, Kissel T, Quante J and Matusch R 1980 *Chem. Ber.* **113** 1898
[70] Mizuno M, Garito A and Cava M 1978 *J. Chem. Soc. Chem. Commun.* **1978** 18
[71] Gärtner S, Schweitzer D and Keller H J 1991 *Synth. Met.* **44** 227
[72] Grießhaber E 2000 *PhD Thesis* University of Stuttgart, German
[73] Barron T H K, Collins J G and White G K 1980 Thermal expansion of solids at low temperatures *Adv. Phys.* **29** 609–730
[74] de Souza M, Foury-Leylekian P, Moradpour A, Pouget J-P and Lang M 2008 *Phys. Rev. Lett.* **101** 216403
[75] de Souza M, Brühl A, Strack C, Wolf B, Schweitzer D and Lang M 2007 *Phys. Rev. Lett.* **99** 037003
[76] Manna R S, de Souza M, Bruehl A, Schlueter J A and Lang M 2010 *Phys. Rev. Lett.* **104** 016403
[77] Manna R, Wolf B, de Souza M and Lang M 2012 *Rev. Sci. Instrum.* **83** 085111
[78] Pregelj M *et al* 2010 *Phys. Rev.* B **82** 144438
[79] Jesche A, Krellner C, de Souza M, Lang M and Geibel C 2010 *Phys. Rev.* B **81** 134525
[80] Jesche A *et al* 2012 *Phys. Rev.* B **86** 020501
[81] de Souza M, Hofmann D, Foury-Leylekian P, Moradpour A, Pougetb J-P and Lang M 2010 *Physica* B **405** S92
[82] Jesche A, Krellner C, de Souza M, Lang M and Geibel C 2009 *New J. Phys.* **11** 103050
[83] de Souza M, Haghighirad A-A, Tutsch U, Assmus W and Lang M 2010 *Eur. Phys. J.* B **77** 101
[84] de Souza M and Pouget J-P 2013 *J. Phys.: Condens. Matter* **25** 343201
[85] de Souza M, Brühl A, Strack C, Schweitzer D and Lang M 2012 *Phys. Rev.* B **86** 085130
[86] Kund M, Mtiller H, Kushch N D, Andres K and Saito G 1995 *Synth. Met.* **70** 951
[87] Pott R and Schefzyk R 1983 *J. Phys.* E **16** 445
[88] Fietz W H, Grube K and Leibrock H 2000 *High Pressure Res.* **19** 373
[89] Köppen M *et al* 1999 *Phys. Rev. Lett.* **82** 4548
[90] Lang M 1991 *PhD Thesis* Darmstadt Technical University, Darmstadt, German
[91] Müller J 2001 *PhD Thesis* Max-Planck-Institute, Dresden, Germany
[92] Brühl A 2007 *PhD Thesis* University of Frankfurt, Frankfurt, Germany
[93] Loram J W, Mirza K A, Joyce C P and Osborne A J 1989 *Europhys. Lett.* **8** 263
[94] Chasseau D 1991 *Synth. Met.* **42** 2039
[95] Toyota N, Watanabe Y and Sasaki T 1993 *Synth. Met.* **55** 2536
[96] Lakes R 1987 *Sience* **235** 1038
[97] Wolter A U B, Feyerherm R, Dudzik E, Süllow S, Strack C, Lang M and Schweitzer D 2007 *Phys. Rev.* B **75** 104512
[98] Goodwin A L, Calleja M, Conterio M J, Dove M T, Evans J S O, Keen D A, Peters L and Tucker M G 2008 *Science* **319** 794
[99] Goodwin A L and Kepert C J 2005 *Phys. Rev.* B **71** 140301
[100] de Souza M *et al* unpublished results
[101] Evans J S O 1999 *J. Chem. Soc. Dalton Trans.* **19** 3317
Barrera G D, Bruno J A O, Barron T H K and Allan N L 2005 *J. Phys.: Condens. Matter* **17** R217
[102] Mary T A, Evans J S O, Vogt T and Sleight A W 1996 *Science* **272** 90
[103] Roth S 1995 *One-Dimensional Metals* (Germany: VCH)
[104] Müller J *et al* 2000 *Phys. Rev.* B **61** 11739
[105] Pouget J-P and Ravy S 1984 *J. Phys.* I **6** L393
[106] Elsinger H, Wosnitza J, Wanka S, Hagel J, Schweitzer D and Strunz W 2000 *Phys. Rev. Lett.* **84** 6098
[107] Nakazawa Y, Taniguchi H, Kawamoto A and Kanoda K 2000 *Phys. Rev.* B **61** R16295

[108] Lang M, de Souza M, Brühl A, Strack C, Wolf B and Schweitzer D 2008 *Physica* B **403** 1384
[109] Taniguchi H, Kawamoto A and Kanoda K 1999 *Phys. Rev.* B **59** 8424
[110] Blundell S 2001 *Magnetism in Condensed Matter* (Oxford: Oxford University Press)
Pankhurst Q A, Johnson C E, Jones D H and Thomas M E 1988 *Hyperfine Interact.* **41** 505
[111] Ramirez A P, Hayshi A, Cava R J, Siddharthan R and Shastry B S 1999 *Nature* **399** 333
[112] Taniguchi H *et al* 2003 *Phys. Rev.* B **67** 014510
[113] Zhang S-C 1997 *Science* **275** 1089
[114] Georges A *et al* 1996 *Rev. Mod. Phys.* **68** 13
[115] Smith D F 2000 *Phys. Rev.* B **68** 024512
[116] Pauling L 1935 *J. Am. Chem. Soc.* **57** 2680
[117] Pankhurst Q A, Johnson C E, Jones D H and Thomas M F 1988 *Hyperfine Interact.* **41** 505
[118] Su X, Zuo F, Schlueter J A, Kini A M and Williams J M 1998 *Phys. Rev.* B **58** R2944
[119] Griesshaber E, Schiller M, Schweitzer D, Heinen I and Strunz W 1999 *Physica* C **317** 421
[120] Huang K 1987 *Statistical Mechanics* (New York: Wiley)
[121] Goldenfeld N 1992 *Lectures on Phase Transitions and the Renormalization Group* (Reading, MA: Addison-Wesley)
[122] Cardy J L 1996 *Scaling and Renormalization in Statistical Physics* (Cambridge: Cambridge University Press)
[123] Kardar M 2007 *Statistical Physics of Fields* (Cambridge: Cambridge University Press)
[124] Kopietz P, Bartosch L and Schütz F 2010 *Introduction to the Functional Renormalization Group* (Berlin: Springer)
[125] Levanyuk A P 1959 *Zh. Eksperim. i Teor. Fiz.* **36** 810
Levanguk A P 1959 *Sov. Phys.—JETP* **9** 571 (Engl. transl.)
[126] Ginzburg V L 1960 *Fiz. Tverd. Tela.* **2** 2031
Ginzburg V L 1960 *Sov. Phys.–Solid State* **2** 1824 (Engl. transl.)
[127] Limelette P, Georges A, Jerome D, Wzietek P, Metcalf P and Honig J M 2003 *Science* **302** 89
[128] LaBella V P, Bullock D W, Anser M, Ding Z, Emery C, Bellaiche L and Thibado P M 2000 *Phys. Rev. Lett.* **84** 4152
[129] Lipa J A, Swanson D R, Nissen J A, Chui T C P and Israelsson U E 1996 *Phys. Rev. Lett.* **76** 944
[130] Pelissetto A and Vicari E 2002 *Phys. Rep.* **368** 549
[131] Campostrini M, Hasenbusch M, Pelissetto A and Vicari E 2006 *Phys. Rev.* B **74** 144506
[132] Campostrini M, Hasenbusch M, Pelissetto A, Rossi P and Vicari E 2002 *Phys. Rev.* B **65** 144520
[133] Onsager L 1944 *Phys. Rev.* **65** 117
[134] Kadanoff L P, Götze W, Hamblen D, Hecht R, Lewis E A S, Palciauskas V V, Rayl M and Swift J 1967 *Rev. Mod. Phys.* **39** 395–431
[135] Imada M 2005 *Phys. Rev.* B **72** 075113
[136] Imada M, Misawa T and Yamaji Y 2010 *J. Phys.: Condens. Matter* **22** 164206
[137] Castellani C, Di Castro C, Feinberg D and Ranninger J 1979 *Phys. Rev. Lett.* **43** 1957
[138] Fonseca P and Zamolodchikov A 2003 *J. Stat. Phys.* **110** 527
[139] Zhu L, Garst M, Rosch A and Si Q 2003 *Phys. Rev. Lett.* **91** 066404
[140] Kotliar G, Lange E and Rozenberg M J 2000 *Phys. Rev. Lett.* **84** 5180
[141] Fujita A, Suzuki T, Kataoka N and Fukamichi K 1994 *Phys. Rev.* B **50** 6199
[142] Schlesinger Z, Rosen J A, Hancock J N and Ramirez A P 2008 *Phys. Rev. Lett.* **101** 015501
[143] Sémon P and Tremblay A-M S 2012 *Phys. Rev.* B **85** 201101
[144] Kokalj J and McKenzie R H 2014 arXiv:1411.1085